Schildgen, T. F., Cosentino, D., Bookhagen, B., Niedermann, S., Yı,ldı,rı,m, C., Echtler, H., Wittmann, H., Strecker, M. R. (2012): Multi-phased uplift of the southern margin of the Central Anatolian plateau, Turkey: A record of tectonic and upper mantle processes. - Earth and Planetary Science Letters, 317-318, 85-95

DOI: 10.1016/j.epsl.2011.12.003

Multi-phased uplift of the southern margin of the Central Anatolian plateau, Turkey: A record of tectonic and upper mantle processes

Earth and Planetary Science Letters (2012), *doi: 10.1016/j.epsl.2011.12.003*

T.F. Schildgen[a*], D. Cosentino[b,c], B. Bookhagen[d], S. Niedermann[e], C. Yıldırım[e], H. Echtler[e,a], H. Wittmann[e], M.R. Strecker[a]

[a] Institut für Erd-und Umweltwissenschaften and DFG-Leibniz Center for Earth Surface and Climate Studies, Potsdam University, Karl-Liebknecht-Str. 24, Haus 27, 14476 Potsdam-Golm, Germany
[b] Dipartimento di Scienze Geologiche, Università degli Studi Roma Tre, Largo San Leonardo Murialdo 1, 00146 Rome, Italy
[c] Istituto di Geologia Ambientale e Geoingegneria (IGAG-CNR) Area della Ricerca Roma 1 Montelibretti, Via Salaria Monterotondo Scalo, 00016 Rome, Italy
[d] Department of Geography, 1832 Ellison Hall, University of Santa Barbara, Santa Barbara, CA 93106-4060, USA
[e] Helmholtz-Zentrum Potsdam, Deutsches GeoForschungsZentrum (GFZ), Telegrafenberg, 14473 Potsdam, Germany

Abstract

Uplifted Neogene marine sediments and Quaternary fluvial terraces in the Mut Basin, southern Turkey, reveal a detailed history of surface uplift along the southern margin of the Central Anatolian plateau from the Late Miocene to the present. New surface exposure ages (^{10}Be, ^{26}Al, and ^{21}Ne) of gravels capping fluvial strath terraces located between 28 and 135 m above the Göksu River in the Mut Basin yield ages ranging from ca. 25 to 30 ka, corresponding to an average incision rate of 0.52 to 0.67 mm/yr. Published biostratigraphic data combined with new interpretations of the fossil assemblages from uplifted marine sediments reveal average uplift rates of 0.25 to 0.37 mm/yr since Late Miocene time (starting between 8 and 5.45 Ma), and 0.72 to 0.74 mm/yr after 1.66 to 1.62 Ma. Together with the terrace abandonment ages, the data imply 0.6 to 0.7 mm/yr uplift rates from 1.6 Ma to the present. The different post-Late Miocene and post-1.6 Ma uplift rates can imply increasing uplift rates through time, or multi-phased uplift with slow uplift or subsidence in between. Longitudinal profiles of rivers in the upper catchment of the Mut and Ermenek basins show no apparent lithologic or fault control on some knickpoints that occur at 1.2 to 1.5 km elevation, implying a transient response to a change in uplift rates. Projections of graded upper relict channel segments to the modern outlet, together with constraints from uplifted marine sediments, show that a slower incision/uplift rate of 0.1 to 0.2 mm/yr preceded the 0.7 mm/yr uplift rate. The river morphology and profile projections therefore reflect multi-phased uplift of the plateau margin, rather than steadily increasing uplift rates. Multi-phased uplift can be explained by lithospheric slab break-off and possibly also the arrival of the Eratosthenes Seamount at the collision zone south of Cyprus.

1. Introduction

Understanding the history of surface uplift at an orogen scale is among the most challenging tasks in the geosciences, particularly in terms of identifying the roles of crustal versus mantle processes in producing and maintaining high topography. Paleoaltimetry studies have demonstrated that the magnitude of surface uplift can often only be estimated with large uncertainties (Quade et al., 2007; Riihimaki and Libarkin, 2007; Sahagian and Proussevitch, 2007). Higher precision estimates have been derived from uplifted, datable marine and terrestrial reference surfaces (Abbott et al., 1997; Bookhagen et al., 2006a; Cosentino and Gliozzi, 1988; Cosentino et al., 2009; Dethier et al., 1995; Gardner et al., 1992; Jordan et al., 2010; Melnick et al., 2009; Merritts and Bull, 1989; Perg et al., 2001; Westaway, 1993; Zazo et al., 2003), from fluvial strath terraces (Lavé and Avouac, 2001; Pazzaglia and Brandon, 2001; Schildgen et al., 2009a; Seyrek et al., 2008; Wegmann and Pazzaglia, 2009; Westaway et al., 2004), and from river incision through regional paleosurfaces (Clark et al., 2005; Gubbels et al., 1993; Schildgen et al., 2007, 2009b). River longitudinal profiles are also increasingly being used to infer changes in uplift (Barke and Lamb, 2006; Harkins et al., 2007; Hilley and Arrowsmith, 2008; Hoke et al., 2007; Kirby et al., 2003; Molin et al., 2004; Seeber and Gornitz, 1983; Wobus et al., 2006). Where channel forms can be calibrated to erosion or uplift rates, they

can be used to semi-quantitatively assess changes in uplift rates through time or space (Duvall et al., 2004; Kirby and Whipple, 2001; Lague and Davy, 2003; Snyder et al., 2000).

The southern margin of the Central Anatolian plateau (Fig. 1) is ideally suited for surface uplift studies spanning multiple timescales. Miocene marine sediments onlap basement rocks at elevations up to 2 km (Cosentino et al., in press), and Early Pleistocene marine sediments crop out as high as 1.2 km (Yıldız et al., 2003). In the same area, fluvial strath terraces that are preserved between 28 and 135 m above the Göksu River record the most recent river incision. However, the details of the younger uplift history and the mechanisms underlying regional uplift are not yet well understood. The Anatolian plateau lies at the intersection of a complex tectonic regime, just north of the triple junction between the Arabian, African, and Eurasian plates (Fig. 1), where modern topography has likely integrated the effects of both tectonic processes (Clark and Robertson, 2002, 2005; Jaffey and Robertson, 2005; Robertson et al., 2009; Şengör and Yılmaz, 1981) and upper mantle processes (Faccenna et al., 2006; Keskin, 2003; Şengör et al., 2003). As such, it represents an ideal testing ground for discerning the nature of geodynamic processes through reconstructions of surface uplift.

Our multidisciplinary approach to exploring surface uplift at the southern margin of the Central Anatolian plateau utilizes uplifted marine sediments, fluvial strath terraces, and river profile analysis. We report the first strath terrace abandonment ages from the region using cosmogenic ^{10}Be, ^{26}Al, and ^{21}Ne exposure dating of fluvial gravels capping the terraces. Ages of uplifted marine successions are derived from published data (Cosentino et al., in press; Yıldız et al., 2003) as well as our reinterpretations of microfossil assemblages originally reported by Yıldız et al. (2003). We use uplift constraints from the marine sediments and fluvial terraces to semi-quantitatively assess uplift rates that are recorded in relict portions of channel profiles throughout our study area. Our integrated approach provides an unprecedented look into surface uplift of the southern plateau margin over multiple timescales, as well as clues to the mechanisms underlying uplift and plateau development.

2. Regional deformation and uplift

The modern topography of the Central Anatolian plateau is the result of crustal-scale deformation with probable contributions from mantle and lithospheric-scale processes. The Central Taurides, which define the plateau's southern margin (Fig. 1), were accreted to crustal blocks to the north starting in the Eocene (Jaffey and Robertson, 2005; Pourteau et al., 2010; Robertson et al., 1996; Şengör and Yılmaz, 1981; Şengör et al., 1984, 1985; Yılmaz et al., 1997), while closure of the Neotethys Ocean to the south and associated Arabia–Eurasia collision (Ballato et al., 2011; Hüsing et al., 2009; Kelling et al., 1987; Robertson, 2000; Şengör et al., 1985; Williams et al., 1995) resulted in westward "escape" of the Anatolian microplate along the North and East Anatolian faults (Dewey and Şengör, 1979; Şengör et al., 1985). Some uplift of Central Anatolia likely resulted from this plate-scale deformation, both along the southern margin prior to the Middle Miocene (Clark and Robertson, 2002, 2005;Jaffey and Robertson, 2005) and at the northern margin due to strain accumulation along the broad restraining bend of the North Anatolian Fault (Yıldırım et al., 2011).

Beyond these crustal-scale processes, seismic evidence for a thin or absent mantle lithosphere beneath Eastern Anatolia (Al-Lazki et al., 2003, 2004; Gök et al., 2003, 2007; Lei and Zhao, 2007) and regional volcanism close to the presumed onset of uplift (Pearce et al., 1990) inspired suggestions that slab steepening, delamination, and break-off induced Late Miocene uplift of Eastern Anatolia (KIeskin, 2003; Şengör et al., 2003). P-wave seismic tomography in Central Anatolia is consistent with a slab break-off beneath Eastern Anatolia extending as far west as the longitude of Cyprus (Biryol et al., 2011; Gans et al., 2009) with a potential tear between the Cyprean and Aegean slabs (Biryol et al., 2011); subsequently, delamination (Bartol et al., 2011) and slab break-off (Cosentino et al., in press) have been suggested to explain surface uplift since the Late Miocene in Central Anatolia as well.

An additional phase of deformation affected the easternmost Medterranean (Cyprus, and areas to the north and east) since Early to Middle Pleistocene time (Harrison et al., 2008; Kinnaird et al., 2011; Robertson, 1998; Schattner, 2010). The timing is broadly coincident with the arrival of the Eratosthenes seamount in the collision zone south of Cyprus, which currently separates the Eurasian (Anatolian) and African plates.

3. Setting of the Göksu River and the Mut Basin

The Göksu River, with its 11,200 km^2 drainage basin, is the largest river that crosses the southern margin of the Central Anatolian plateau. Along its course across the margin through the Mut Basin (Fig. 2), the river has exposed Oligocene to Early Miocene continental sediments and Miocene to Pleistocene marine sediments that unconformably overlie Mesozoic and older basement lithologies. Cosentino et al. (in press) reported a biostratigraphic age of ca. 8 Ma for marine sediments that cap the southern plateau margin at ca. 2 km elevation near the town of Basyayla, revising estimates that marine sedimentation had continued through at least Langhian (16 to 13.6 Ma, Bassant et al., 2005) or Serravallian (13.6 to 11.6 Ma, Tanar and Gökçen, 1990)

time. The Late Miocene marine sediments are warped into a broad, 100-km wide drape fold, with minor dip-slip and oblique normal faulting (Cosentino et al., in press). The start of uplift can probably be further limited by the 5.45 Ma onset of rapid subsidence and sedimentation in the Adana Basin (Cosentino et al., 2010), south of the uplifted margin (Fig. 1). Considering that both ages limit the start of uplift to between 8 and 5.45 Ma, the margin experienced an average long-term uplift rate of 0.25 to 0.37 mm/yr.

Southeast of the town of Mut (Fig. 2), younger marine sediments onlap the Middle to Late Miocene shallow- and deeper-water marine deposits (Mut and Köselerli Formations, respectively). Uplift since deposition of the younger sequence has raised the onlap surface to 1.2 km elevation. Micropaleontological investigations by Yıldız et al. (2003) on these deposits pointed to a Pliocene to Pleistocene sedimentation age, and to a Calabrian age (1.8 to 0.7 Ma) for the highest part of the sections near the villages of Sarıkavak and Hacıahmetli (Fig. 2A).

4. Fluvial terraces of the Mut Basin

Fluvial terraces of the Göksu River record the most recent river incision through the older sedimentary units of the Mut Basin. The terrace surfaces range from 200 to 30,000 m^2 in extent at heights between 28 and 135 m above the modern thalweg, between ca. 150 and 50 km inland from the coast (Fig. 2). We identified terraces based on the occurrence of fluvial gravels of relatively uniform thickness (typically 1.5 to 2.5 m) capping a beveled surface cut into the older sedimentary sequence. These relatively thin gravels likely represent the mobile alluvial cover of a bedrock channel (Pazzaglia and Brandon, 2001), which would imply that the beveled surfaces beneath the gravels are "strath" terraces (Bull, 1991). No similar deposits were identified within the older stratigraphy, except near the basin margins, where finer grained sediments transition to coarse sandstones and pebbles. The fluvial gravels are dominated by carbonate clasts, with rare occurrences (ca. 1%) of red chert. The gravels are generally well-cemented, except for the lowest terrace gravels, which show carbonate accumulations on the undersides of clasts. Although most of the gravels are not covered by finer sediments, in the central portion of some terraces there is a ca. 10 to 30 cm thick deposit of fine-grained sand and silt, which may be the remnant of an overbank deposit.

The low (28 to 34 m) and intermediate (ca. 50 to 100 m) terraces exhibit relatively smooth, flat surfaces of cemented river gravels (Fig. 3A) generally 1.5 to 2.5 m thick. Preservation of the gravels seems primarily controlled by erosion of the relatively soft sediments beneath them, which results in the overlying gravels breaking off in blocks. In contrast, the 110-m terrace gravels (sample 09MUT17) are cemented, but with an irregular surface (Fig. 3B), a reduced thickness (ca. 0.5 to 1 m) and a higher concentration of chert (ca. 10%) compared to the lower terrace gravels, suggesting that the surrounding carbonates may have been dissolved. The highest sample site (135 m, 09MUT18) contained no cemented gravels, but was a cultivated surface with sparse, rounded chert clasts.

5. Methods and approaches

5.1. Samples for cosmogenic nuclide analysis

We collected chert samples for cosmic ray exposure dating (^{10}Be, ^{26}Al, and ^{21}Ne) from the surfaces of gravel deposits overlying fluvial straths. Single amalgamated samples from each surface consisted of 30 to 50 clasts between 1 and 3 cm in diameter, which should represent the mean surface concentration (Repka et al., 1997). Details of sample processing are given in the Supplementary material. Accelerator mass spectrometry measurements were made at Lawrence Livermore National Laboratory. We rely on the original ICN standard (Nishiizumi et al., 2007). We calculated surface ages using the Cronus online calculator version 2.2.1 (available at http://hess.ess.washington.edu/, with documentation in Balco et al., 2008), which includes variations in altitude, latitude, and topographic shielding in calculating production rates from spallation and muons, and assumes reference ^{10}Be production rates that depend on the selected scaling scheme (Balco et al., 2008). Errors in the reference production rates are estimated at ca. 10% (Balco et al., 2008). Table A1 lists sample input parameters and measured ^{10}Be and ^{26}Al concentrations with analytical errors. Ages based on various production rate scaling schemes are summarized in Table A2. Although seasonal snow cover can shield surfaces from cosmogenic nuclide accumulation (Schildgen et al., 2005), such effects are insignificant at low elevations of the Eastern Mediterranean. We calculated ^{21}Ne production rates using a value of 0.232 ± 0.009 for the ratio of ^{10}Be/^{21}Ne production (Goethals et al., 2009) to correspond to a 1.387 Ma ^{10}Be half-life (Chmeleff et al., 2010; Korschinek et al., 2010), and using the ^{10}Be production rates derived from the Lal (1991)/Stone (2000) constant production rate scaling with a total reference ^{10}Be production rate (from spallation and muon production) of 4.58 ± 0.43 atoms/(g yr). Stepwise heating Ne data are given in Table A3, and ^{21}Ne ages are summarized in Table A4.

In calculating corrections to exposure ages related to erosion of material above the sampled surfaces, we considered the relationship

$$P(x) = P_n(0)\exp\left[\frac{-\rho x}{\Lambda_n}\right] + P_\mu(0)\exp\left[\frac{-\rho x}{\Lambda_\mu}\right] \quad (1)$$

where P(x) is production at depth × (cm), $P_n(0)$ is the surface production rate for neutron spallation (atoms/(g yr)), ρ is the density of the overlying material (g/cm^3), P (0) is the surface production rate for muons (atoms/(g yr)), calculated to be ca. 4% of total production at surface using Cronus (version 2.2.1), Λ_n is the attenuation length for fast neutrons (160 g/cm^2, Balco et al., 2008), and Λ_μ is the attenuation length for muons. We combined the contributions from negative muons and fast muons, as both can be reasonably described with an attenuation length of 1500 g/cm^2 in the upper ca. 10 m of rock (Gosse and Phillips, 2001).

5.2. River profiles

Across a wide range of tectonic and climatic settings, river channels tend to be characterized by the scaling relationship

$$S = k_s A^{-\theta} \quad (2)$$

where S is the slope (m/m), k_s is the steepness index (m$^{2\theta}$), A is the drainage area (m^2), and θ is the concavity (Flint, 1974). Normalized steepness index values (k_{sn}) are steepness indexes calculated using a reference concavity (θ_{ref}). An increase in uplift rate will produce a downstream increase in the channel gradient, and the "knickpoint" separating downstream and upstream reaches should migrate up-stream in a kinematic wave (Rosenbloom and Anderson, 1994). The downstream portion of the channel, which is adjusted to the new uplift rate, is typically characterized by a higher k_s (e.g., Snyder et al., 2000). In areas of relatively uniform climate and lithology and no dependence of θ on uplift rate, the vertical component of knickpoint migration should be constant (Niemann et al., 2001). Observing knickpoints at a similar elevation within a drainage network is, there- fore, one line of evidence to support a past base level drop or increase in uplift rate (Crosby and Whipple, 2006; Wobus et al., 2006).

We extracted river profiles from 90-m resolution Shuttle Radar Topography Mission (SRTM) digital elevation model (DEM) data (Jarvis et al., 2008) using the Stream Profiler tool, available at www.geomorphtools.org, with procedures described in Wobus et al. (2006). Projection of the original DEM into the Universal Transverse Mercater (UTM) system yielded a final pixel size of 110 × 110 m.

Because graded rivers have adjusted their incision rates to match the background uplift rate, a simple scaling relationship exists between the change in channel elevations (ΔZ) upstream from a knickpoint and the uplift rates prior to (U_f) and following (U_f) a sudden increase in uplift (Whipple, 2001; Whipple and Tucker, 1999):

$$\Delta Z = \Delta t\left(U_f - U_i\right) \quad (3)$$

where Δt is the time elapsed since the change in uplift rate. In essence, the upper portion of the channel is passively uplifted at the new uplift rate, but continues to incise at a rate that was set by the initial uplift rate. We projected upper channel segments to the modern outlet to determine ΔZ, such that we could explore relationships between U_f and U_i (Fig. %C).To make this projection, we first applied the scaling relationship in Eq. (2) using the k_s and θ of the upstream channel section (derived from a curve fit of slope versus area data) and the drainage area along the modern channel to calculate the slopes along a projection of the upper channel; we then used the slopes to determine successive drops in channel elevation down- stream from the knickpoint. Our final ranges of projected heights at the outlet incorporate the best-fit θ value and 2σ errors in k_s. We selected channels for projection throughout the catchment that had the lowest errors on k_s (based on the curve fit of the slope versus area data) to find representative but precise estimates for Δ Z.

6. Results

6.1. Age of the youngest marine sediments in the Mut Basin

Yıldız et al. (2003) reported two stratigraphic sections containing Pleistocene marine deposits close to the villages of Sarıkavak (600–650 m) and Hacıahmetli (1165 m) (Fig. 2A). Near Sarıkavak, the highest four samples in the section contain marker species for defining the age of the youngest marine sediments in the area. In the reported list of the microfossils, it is worthy to note the occurrence of Globigerinoides tenellus in the planktonic foraminifera assemblages, and Calcidiscus macintyrei, Gephyrocapsa caribbeanica and Gephyrocapsa oceanica (medium Gephyrocapsa) in the calcareous nannofossil assemblages. In the Neogene Mediterranean biozonation (Iaccarino et al., 2007) the first occurrence (FO) of G. tenellus is at the base of the Globigerina cariacoensis Zone (1.79–0.94 Ma, Lourens et al., 2004), which defines the Calabrian stage of the Early Pleistocene. The occurrence of both C. macintyrei and medium Gephyrocapsa allow us to better constrain the age of the top of the Sarıkavak section. Because the FO of medium Gephyrocapsa is at 1.73 Ma (Raffi, 2002) and the last occurrence (LO) of C. macintyrei is calibrated at 1.66 Ma (Lourens et al., 2004), the Calabrian deposits of the Sarıkavak section should have ages between 1.73 and 1.66 Ma.

The reported microfossil associations from the Hacıahmetli section include no planktonic foraminifera, although calcareous nannofossil assemblages were found in four out of five collected samples. The lowermost sample of the Hacıahmetli section still contains C. macintyrei, whereas in the upper part of the section, together with small Gephyrocapsa, only Calcidiscus leptoporus were found. According to the calcareous nannofossil biochronology, the top of the Hacıahmetli section should be younger than the LO of C. Macintyrei and older than the FO of large Gephyrocapsa (1.62 Ma, Lourens et al., 2004). The uppermost marine deposits of the Hacıahmetli section are younger than the Calabrian sediments at the top of the Sarıkavak section, and have ages between 1.66 and 1.62 Ma. Importantly, these youngest marine sediments, with their modern elevation of ca. 1.2 km, point to a surface uplift rate of 0.72 to 0.74 mm/yr after 1.66 to 1.62 Ma.

6.2. Exposure ages of gravels capping fluvial strath terraces

The exposure ages of the terrace-capping gravels cluster into two main groups: gravels between 28 and 34 m above the river are ca. 20 and 40 ka and those between 40 and 135 m above the river are ca. 70 to 130 ka (Table A2, Fig. 4). These clusters correspond to relative sea level high stands during Marine Isotope Stages 3 and 5 (Fig. 4). Al-though erosion may have reduced the exposure ages of all the gravels, the highly degraded nature of the two highest gravel units (09MUT17 and 09MUT18) implies that they are the most severely affected, and may yield ages much younger than their true ages.

The relatively large uncertainties on ^{21}Ne ages are related to high concentrations of ^{20}Ne, resulting in small excesses of ^{21}Ne/ ^{20}Ne in the 400 and 600 °C temperature steps (Table A3). Samples analyzed for ^{21}Ne were also analyzed for ^{10}Be and/or ^{26}Al. Sample 09MUT12 shows similar ^{10}Be, ^{26}Al, and ^{21}Ne ages, but the ^{21}Ne age of 08TSERM04 is significantly older than its ^{10}Be age. That ^{21}Ne age is also the single old outlier within the dataset, which we have removed from our curve-fitting analysis. For 09MUT08, the ^{26}Al age overlaps within error of the ^{21}Ne age. This correspondence suggests that the sample may be a young outlier in the dataset, possibly as a result of surface erosion. During the stepwise heating of 09MUT08 and

09MUT12, both the total Ne concentrations and the ^{21}Ne excesses were very low above 600 °C (Table A3), indicating that nucleogenic ^{21}Ne is insignificant and our concentration estimates for cosmogenic ^{21}Ne are robust within the stated error limits. In contrast, 08TSERM04 released ~35% of the total ^{21}Ne excess in the 800 °C step, so we can- not exclude a nucleogenic ^{21}Ne contribution for this sample.

Excluding the two highest samples and the single old ^{21}Ne result, we used the remaining ages and heights to determine average river incision rates. We applied a York (1969) linear regression, including errors in calculated terrace abandonment ages (“external” uncertainties from the Cronus online calculator, Balco et al., 2008) and in measurements of terrace gravel height. Because different cosmogenic production rate scaling schemes yield slightly different calculated

6.3. Potential errors and corrections on exposure ages

Surface erosion and nuclide inheritance complicate interpretations of cosmogenic exposure ages of landforms (Anderson et al., 1996; Nishiizumi et al., 1986). Carbonate cementation of the gravels is likely to have helped protect the gravel surfaces from postdepositional erosion. However, as carbonate is deposited first on the undersides of clasts, then progresses to fill voids within a deposit, meteoric water percolation is reduced, resulting in facilitated removal of any overlying material (Gile et al., 1966) and lower calculated exposure ages. Nonetheless, the ages should not be simply interpreted as minimum ages, as nuclides that accumulate in the

gravels during exhumation and transport through the catchment ("inherited" nuclides) have the opposite effect of increasing calculated ages (Repka et al., 1997).

We can estimate a maximum correction for erosion (or shielding) by assuming that overbank material was removed just prior to sampling, hence applying Eq. (1) to compare surface production rates to rates beneath the surface. Correcting for the removal of 0.3 m of overbank material with a density of 1.8 g/cm3 would decrease the production rates, and thus increase all ages by 28%, raising the ages of the lower terrace gravels by 7 to 10 ka and those of intermediate gravels by 24 to 31 ka. A larger correction would be necessary for the highly degraded, two highest terrace gravels. For example, if 1 or 2 m of 2.0 g/cm3 gravels were removed from above those samples just prior to sampling, ages would increase by 69% or 89%, respectively. Nuclide inheritance can be assessed with depth profiles beneath a landform surface, as deep samples are largely shielded from postdepositional nuclide production (Anderson et al., 1996). The cementation of the gravels and rare occurrence of chert in the Mut Basin precluded such sampling. However, we can explore the inherited component of a four-sample depth profile (0- to 2-m-deep) from gravels capping a terrace 150 m above the thalweg near the city of Adana (Supplementary material Fig. A1, "ZIY" samples in Table A1).

To do this, we modeled fits to the depth profile following the approach of Braucher et al. (2003), testing reasonable values for erosion rate (5 to 12 m/Myr), surface age (50 to 300 ka), total erosion of the surface (b1 m), and deposit density (1.8 to 2.0 g/cm^3). Over the full range of erosion rates, χ^2 values were minimized for an inherited component between ca. 88,200 and 91,100 ^{10}Be atoms/g (Table A5). If the inherited components are broadly similar for the two neighboring catchments, we can use the modeled inheritance of the Adana terrace to estimate a correction of 18.8 to 20.6 ka for the Mut Basin terraces.

Changes in terrace abandonment ages would be greatest if there were erosion with no nuclide inheritance, or nuclide inheritance with no erosion. Both scenarios are highly unlikely. We therefore consider that the estimated corrections should at least partly cancel one another. Furthermore, the general simplicity of the age–height relationships of the uncorrected ages suggests that the magnitude of net corrections is relatively low. Considering the possible corrections to the ages, low and intermediate gravels still likely fall within Marine Isotope Stages 3 and 5, and the highest gravels may fall within Stage 7. Hence, the average slope of the age versus height plot (i.e., the incision rate) of 0.52 to 0.67 mm/yr is probably a fairly robust estimate of the latest Pleistocene to recent incision rates.

6.4. River profiles and channel projections

Most river profiles in the Mut Basin and the neighboring Ermenek Basin are characterized by downstream portions with high k_{sn} values (e.g., >90 for θ_{ref}=0.45) that are separated by one or more knickpoints from upper sections with low k_{sn} values (e.g., <60 for θ_{ref} =0.45) (Fig. 5A). We consider a single knickpoint separating these two channel segments to be a "major" knickpoint. Throughout the catchment, major knickpoints generally occur at 1.2 to 1.5 km elevation (Fig. 5B). They often correspond to the lithologic contact between the limestone caprock (Mut Formation) and softer marls (Köselerli Formation) or continental clastics beneath (Fig. 5A, Supplementary material Fig. A2). Major knickpoints along streams in the upper parts of the catchment, which incise through Mesozoic basement carbonates, also occur at elevations of ca. 1.2 to 1.5 km. These latter knickpoints do not appear to have any lithologic or fault control (Fig. 5A) as the knickpoints do not align with any lithologic contacts or tectonic structures. Downstream projections of the upper "relict" portions of channels above the knickpoints show variable results. Streams that incise through the Mut Formation limestone have concavities ranging from 0.42 to 0.80 and project to heights of 1145 to 1408 m above the modern outlet, while streams in the upper catchment that incise only basement have concavities of 0.51 to 0.70 and project to heights of 950 to 1197 m above the outlet (Fig. 5C, Table 1). Considering the scaling relationship between uplift rates and changes in the relict channel elevation (Eq. 3), we can use the projected heights above the outlet (ΔZ) to estimate initial uplift rates (U_i) prior to the onset of faster uplift at ca. 1.6 Ma. If we assume an uplift rate of 0.74 mm/yr started at 1.63 Ma (based on the marine sediments uplifted to 1.2 km), the relict stream segments on the Mut Formation yield a range of U_i between –0.13 and 0.03 mm/yr, and relict streams in the basement yield U_i between 0.00 and 0.15 mm/yr (Table 1).

7. Discussion

7.1. Climatic and tectonic control on river incision and terrace formation

Clustering of the terrace abandonment ages during Marine Isotope Stages 3 and 5 (and possibly also 7) suggests that climate fluctuations associated with sea level oscillations and changes in base level played a role in terrace development. Studies of dated terrace sequences in active tectonic settings worldwide have noted that although sustained surface uplift is required for development of stepped strath terrace sequences, stages of individual terrace formation or abandonment tend to cluster during periods of known climate change (e.g., Bookhagen et

al., 2006b; Bridgland and Westaway, 2008; Bull, 1991; Fuller et al., 1998; Lavé and Avouac, 2001; Merritts et al., 1994; Pan et al., 2003; Pazzaglia and Brandon, 2001; Pazzaglia and Gardner, 1993; Schildgen et al., 2002; Wegmann and Pazzaglia, 2002, 2009).

This clustering likely results from climate-induced changes in sediment and water flux with associated changes between vertical and lateral channel incision, which has been shown to be necessary for strath formation and abandonment (Bogaart et al., 2003; Hancock and Anderson, 2002; Meyer et al., 1995; Tucker and Slingerland, 1997).

Climatic shifts or sea level change as a sole driver for terrace formation and long-term incision can be ruled out based on other dated terrace sequences in the eastern Mediterranean region, which record significantly lower incision rates over a similar time period. For example, along the Ceyhan River of southern Turkey, terraces between 50 and 75 km to the east and southeast of the city of Adana yield incision rates between ca. 0.25 and 0.4 mm/yr since 270 ka (Seyrek et al., 2008). Along the Gediz River in western Turkey, incision rates have been ca. 0.2 mm/yr since Middle Pleistocene time (Westaway et al., 2004). However, in southern Turkey, the similarities between fluvial incision rates (0.52 to 0.67 mm/yr) and post- 1.6 Ma uplift rates constrained by the uplifted marine sediments (0.72 to 0.74 mm/yr) support the notion that relatively fast uplift has characterized the region since 1.6 Ma, and was the main factor driving long-term river incision, despite fluctuations in incision rate that could have resulted from glacial–interglacial cycles.

7.2. Changing uplift rates through time

Considering the elevations of the Late Miocene and Pliocene–Pleistocene marine sediments, the time-averaged uplift rate between 8 and 1.6 Ma was 0.13 mm/yr, and increased to ca. 0.7 mm/yr from ca. 1.6 Ma to the present. However, the marine sediments alone do not allow us to distinguish between surface uplift rates that steadily increased until 1.6 Ma, or multiple phases of uplift with intermittent quiescence or subsidence. The Pliocene–Pleistocene marine sediments in the basin could imply that the region was undergoing subsidence during their deposition, perhaps during a hiatus between different uplift phases. Alternatively, the basin alone may have experienced fault-controlled subsidence while the margin as a whole experienced increasing uplift rates. We observed normal faulting along the basin margin that affected parts of the younger marine succession, although the highest outcrop at 1.2 km elevation lies within the footwall of local normal faults. In yet another scenario, accommodation space may have been created following incision associated with the ca. 1.5 km drawdown of the Mediterranean Sea during the Messinian Salinity Crisis (5.96 to 5.33 Ma, e.g., Clauzon et al., 1996; Krijgsman et al., 1999) and associated isostatic effects (e.g., Govers, 2009). The latter scenario would imply that the Pliocene–Pleistocene section is at least partly a transgressive depositional sequence. River profiles offer a test of the multi-phased uplift versus increasing uplift rate scenarios. To a first order, major knickpoints along river channels that are not controlled by faults or lithologic contacts imply that incision rates must have increased at some point in the past (Whipple and Tucker, 1999). The common occurrence of knickpoints at the lithologic contact between the Mut limestone and the underlying marls suggests we should use caution in interpreting uplift rates derived from those channels. The basement channels, however, show no alignment of knickpoints with lithologic contacts or faults (Fig. 5A); they are thus more likely to reflect a transient incision/uplift signal.

The change in elevation of graded upper channel segments scales with the final uplift rate minus the initial uplift rate (Eg. 3), offering a semi-quantitative record of uplift rates prior to when they increased. Because the upper channel segments are largely outside of the modern basin, they should reflect uplift of the plateau margin itself, rather than being influenced by any fault-controlled subsidence within the basin. The widely varying projected channel heights demonstrate spatially variable uplift, and/or that the channels used for projection may not all be graded, as is required for the method. Graded channels should yield results that are broadly consistent with the uplift constraints from the marine sediments.

All projections from channels within the Mut Formation yield initial uplift rates that are either negative or much lower than the average 0.13 mm/yr uplift rate for the 8 to 1.6 Ma interval based on the uplifted marine sediments. Negative rates imply channel aggradation, while the very low rates may imply that the karst hydrology associated with the Mut Formation has impacted the ability of those channels to continue incising. Furthermore, the correspondence between the major knickpoints along the channels in the Mut Formation and the limestone caprock edges implies that those channel segments may not be reliable recorders of the pre-1.6 Ma uplift rate.

In contrast, the initial uplift rates derived from basement channels range from 0.00 to 0.15 mm/yr (Table 1). Interestingly, only those two basement channels with concavities of ca. 0.5 yield rates (0.13 to 0.15 mm/yr) that are consistent with constraints from the uplifted marine sediments, while those with higher concavities of 0.60 and 0.70 yield rates that are apparently too low (0.00 to 0.07 mm/yr).

Bedrock channels on uniform lithologies experiencing uniform uplift along their length should theoretically have concavities between 0.35 and 0.6, and most cluster very near 0.45 (Whipple and Tucker, 1999). Higher concavities may indicate that the channels are no longer graded after being affected by a downstream decrease in uplift rate or rock strength, transitions to alluvial conditions, or disequilibrium conditions following a decrease in uplift rates (Whipple, 2004). In summary, the high concavities of several upper channel segments preclude their

use for deriving accurate initial uplift rates, with only a few “ideal” cases (stream channels in non-karstified bedrock with moderate concavity values) where the results from channel projections agree with the stratigraphic constraints on uplift. Nonetheless, we emphasize that both the “ideal” channel projections and the major knickpoints along the basement channels are most consistent with a multi-phased uplift history with slow uplift prior to 1.6 Ma (Fig. 6), rather than steadily increasing uplift rates.

7.3. Uplift mechanisms and predicted surface uplift patterns

Our new data on the stratigraphic and geomorphic evolution of the southern margin of the Central Anatolian plateau can provide insight into the long-term deformation and uplift history of the region. Mechanisms that have been proposed to explain surface uplift in Central Anatolia or surrounding regions have some predictable effects on surface uplift patterns, rates, and magnitudes. For example, slab break-off with or without preceding lithospheric delamination is predicted to produce an asymmetric pattern of rapid km-scale surface uplift (within a few million years) with greatest uplift above the slab break-off (Duretz et al., 2011; Gögüs and Pysklywec, 2008), followed by slow thermal subsidence (on the order of 0.01 mm/yr) as the mantle cools to form new lithosphere (Avigad and Gvirtzman, 2009). Cosentino et al. (in press) pointed out that differences in the onset of surface uplift between Eastern and Central Anatolia are consistent with the lateral propagation rate of slab break-off (e.g., van Hunan and Allen, 2011) from the Bitlis–Zagros suture zone to the Mut Basin. If slab break-off induces changes in mantle flow patterns, this may also produce a distinct phase of uplift related only to mantle flow (e.g., Faccenna and Becker, 2011).

The potential for uplift in southern Turkey resulting from the arrival of the Eratosthenes Seamount at the collision zone south of Cyprus is largely unknown. The seamount itself is underlain by ca. 28 km of continental crust (Aal et al., 2001; Ben-Avraham et al., 2002), Cyprus is underlain by ca. 35 km of continental crust (Makris et al., 1983), and to the southeast of the seamount there is either oceanic crust (Ben-Avraham et al., 2002) or highly attenuated continental crust (Gardosh and Druckman, 2006). The collision zone, which has been described as a N-dipping subduction zone (Woodside, 1977), has been more recently interpreted to be accommodating initial collision between the African and Eurasian plates (Robertson, 1998), possibly as a restraining bend along a continent–continent interface (Harrison et al., 2008). Uplift patterns that result from such a collision likely depend on local plate characteristics, and have not yet been explored in detail. Nonetheless, the prevalent Early to Middle Pleistocene structural modifications in the easternmost Mediterranean (see review by Schattner, 2010), including evidence for increased Pleistocene uplift rates in Cyprus (Kinnaird et al., 2011) and in southern Turkey, are broadly coeval with seamount collision with the trench starting in Early to Middle Pleistocene time. The multi-phased uplift of the southern margin of the plateau revealed by our data helps to limit the possible processes that produced uplift. A single mechanism may be invoked only if it can produce multiple uplift phases; i.e., delamination and/or slab break-off combined with changes in mantle flow patterns that result in distinct uplift phases. Alternatively, delamination and/or slab break-off must be invoked together with surface uplift resulting from collision of the Eratosthenes Seamount south of Cyprus, implying that deformation associated with seamount collision extends at least 250 km northward into southern Turkey.

8. Conclusions

Surface cosmogenic exposure ages of gravels covering strath terraces from the Mut Basin at the southern margin of the Central Anatolian plateau yield an average incision rate of 0.52 to 0.67 mm/yr since ca. 130 ka or potentially since as early as MIS7 (ca. 190 to 245 ka). The incision rate agrees with the average post-1.66 to 1.62 Ma uplift rate of 0.72 to 0.74 mm/yr based on uplifted marine sediments in the same area. The post-1.6 Ma uplift rate is 2 to 3 times faster than the average post-Late Miocene surface uplift rate documented by 8-Ma marine sediments that cap the southern margin of the plateau at ca. 2 km elevation (Cosentino et al., in press) and the onset of rapid sedimentation south of the margin at 5.45 Ma (Cosentino et al., 2010). Our analysis of river profiles throughout the Mut–Ermenek Basin, including both the identification of major knickpoints and channel projections, suggests that a slower phase of uplift of 0.1 to 0.2 mm/yr preceded the start of faster (0.5 to 0.7 mm/yr) uplift and incision at ca. 1.6 Ma. We suggest a multi-phased scenario for growth of the southern margin of the Central Anatolian plateau, involving (1) initial deformation of the Tauride basement that created paleotopography onto which Miocene marine sediments were deposited; (2) a phase of ca. 0.8 km of surface uplift starting between 8 and 5.45 Ma until 1.6 Ma; and (3) a phase of rapid uplift starting at ca. 1.6 Ma that has increased the margin elevation by ca. 1.2 km and likely continues to today. The uplift timing and magnitude can be constrained with the uplifted marine sediments, but they do not reveal the nature of any changes in uplift rates through time. On the basis of our river profile analysis and terrace abandonment ages, uplift clearly proceeded in distinct phases, rather than increasing steadily through time. The ca. 0.8 km uplift may have occurred above delaminated lithospheric mantle (Bartol et al., 2011) and/or slab break-off (Cosentino et al., in press), and the final ca. 1.2 km of uplift could be associated with either Early to Middle Pleistocene collision of the Eratosthenes

Seamount (continental fragment) with the trench south of Cyprus (Robertson, 1998; Schattner, 2010), or uplift associated with modified mantle flow patterns following slab break-off.
Supplementary materials related to this article can be found online at doi:10.1016/j.epsl.2011.12.003.

Acknowledgments

This work is part of the Vertical Anatolian Movements Project (VAMP), funded by the TOPO-EUROPE initiative of the European Science Foundation, with contributions by the Istituto di Geologia Ambientale e Geoingegneria (IGAG-CNR com. TA.P05.009, mod. TA.P05.009.003) and the German Science Foundation (DFG: STR373/ 25-1; EC-138/5-1). TFS was supported by the Leibniz Center for Surface Processes and Climate Studies at Potsdam University (DFG: STR373/20-1) and the Alexander von Humboldt Foundation. BB was supported with grants from NASA (NNX08AG05G) and NSF (EAR 0819874). We thank Enzio Schnabel for performing noble gas analyses, Eric Kirby, Dirk Scherler, Brian Clarke and Angela Landgraf for stimulating discussions, and Bora Rojay and Attila Çiner for logistical help and discussions of regional geology. Alastair Robertson and Mark Brandon provided detailed and constructive reviews that helped to improve the manuscript.

References

Aal, A.A., Barkooky, A.E., Gerrits, M., Meyer, H.-J., Schwander, M., Zaaki, H., 2001. Tectonic evolution of the eastern Mediterranean Basin and its significance for the hydrocarbon prospectivity of the Nile River deepwater area. GeoArabia 6, 363–384.

Abbott, L.D., Silver, E.A., Anderson, R.S., Smith, R., Ingle, J.C., Kling, S.A., Haig, D., Small, E., Galewsky, J., Sliter, W., 1997. Measurement of tectonic surface uplift rate in a young collisional mountain belt. Nature 385, 501–507.

Aksu, A.E., Calon, T.J., Hall, J., Mansfield, S., Yasar, D., 2005. The Cilicia–Adana basin complex, Eastern Mediterranean: Neogene evolution of an active fore-arc basin in an obliquely convergent margin. Mar. Geol. 221, 121–159.

Al-Lazki, A.I., Seber, D., Sandvol, E., Turkelli, N., Mohamad, R., Barazangi, M., 2003. Tomographic Pn velocity and anisotropy structure beneath the Anatolian plateau (eastern Turkey) and the surrounding regions. Geophys. Res. Lett. 30, 8043. doi:10.1029/2003GL017391.

Al-Lazki, A.I., Sandvol, E., Seber, D., Barazangi, M., Turkelli, N., Mohamad, R., 2004. On tomographic imaging of mantle lid velocity and anisotropy at the junction of the Arabian, Eurasian and African Plates. Geophys. J. Int. 158, 1024–1040.

Anderson, R.S., Repka, J.L., Dick, G.S., 1996. Explicit treatment of inheritance in dating depositional surfaces using in situ 10Be and 26Al. Geology 24, 47–51.

Avigad, D., Gvirtzman, Z., 2009. Late Neoproterozoic rise and fall of the northern Arabian–Nubian shield: the role of lithospheric mantle delamination and subsequent thermal subsidence. Tectonophysics 477, 217–228.

Balco, G., Stone, J.O., Lifton, N.A., Dunai, T.J., 2008. A complete and easily accessible means of calculating surface exposure ages or erosion rates from 10Be and 26Al measurements. Quat. Geochronol. 3, 174–195.

Ballato, P., Uba, C.E., Landgraf, A., Strecker, M.R., Sudo, M., Stockli, D.F., Friedrich, A., Tabatabaei, S.H., 2011. Arabia–Eurasia continental collision: insights from late Tertiary foreland-basin evolution in the Alborz mountains, northern Iran. Geol. Soc. Am. Bull. 123, 106–131.

Barke, R., Lamb, S., 2006. Late Cenozoic uplift of the Eastern Cordillera, Bolivian Andes. Earth Planet. Sci. Lett. 249, 350–367.

Bartol, J., Govers, R., Wortel, R., 2011. The Central Anatolian Plateau: relative timing of uplift and magmatism. Geophys. Res. Abstr. 13 (EGU2011-10326).

Bassant, P., van Buchem, F.S.P., Görür, N., 2005. The stratigraphic architecture and evolution of the Burdigalian carbonate–siliciclastic sedimentary systems of the Mut Basin, Turkey. Sediment. Geol. 173, 187–232.

Ben-Avraham, Z., Ginzburg, A., Makris, J., Eppelbaum, L., 2002. Crustal structure of the Levant Basin, eastern Mediterranean. Tectonophysics 346, 23–43.

Bintanja, R., van der Wal, R.S.W., Oerlemans, J., 2005. Modelled atmospheric temperature and global sea levels over the past million years. Nature 437 (7055), 125–128.

Biryol, C.B., Beck, S.L., Zandt, G., Özacar, A.A., 2011. Segmented African lithosphere beneath the Anatolian region inferred from teleseismic p-wave tomography. Geophys. J. Int. 184, 1037–1057.

Bogaart, P.W., Balen, R.T.V., Kasse, C., Vandenberghe, J., 2003. Process-based modelling of fluvial system response to rapid climate change II. Application to the River Maas (The Netherlands) during the last glacial–interglacial transition. Quat. Sci. Rev. 22, 2097–2110.

Bookhagen, B., Echtler, H.P., Melnick, D., Strecker, M.R., Spencer, J.Q.C., 2006a. Using uplifted Holocene beach berms for paleoseismic analysis of the Santa Maria Island, south-central Chile. Geophys. Res. Lett. 33 (15), L15302. doi:10.1029/2008jb005788.

Bookhagen, B., Fleitmann, D., Nishiizumi, K., Strecker, M.R., Thiede, R.C., 2006b. Holocene monsoonal dynamics and fluvial terrace formation in the northwest Himalaya, India. Geology 34, 601–604.

Braucher, R., Brown, E.T., Bourlès, D.L., Colin, F., 2003. In situ produced 10Be measurements at great depths: implications for production rates by fast muons. Earth Planet. Sci. Lett. 211, 251–258.

Bridgland, D., Westaway, R., 2008. Climatically controlled river terrace staircases: a worldwide Quaternary phenomenon. Geomorphology 98, 285–315.

Bull, W.B., 1991. Geomorphic Response to Climatic Change. Oxford University Press, New York. 326 pp.

Chmeleff, J., von Blanckenburg, F., Kossert, K., et al., 2010. Determination of the 10Be half-life by multicollector ICP-MS and liquid scintillation counting. Nucl. Instrum. Methods Phys. Res., Sect. B 268 (2), 192–199.

Clark, M.S., Robertson, A.H.F., 2002. The role of the Early Tertiary Ulukisla Basin, southern Turkey in suturing of the Mesozoic Tethys ocean. J. Geol. Soc. 159, 673–690.

Clark, M., Robertson, A.H.F., 2005. Uppermost Cretaceous–Lower Tertiary Ulukisla Basin, south-central Turkey: sedimentary evolution of part of a unified basin complex within an evolving Neotethyan suture zone. Sediment. Geol. 173, 15–51.

Clark, M.K., House, M.A., Royden, L.H., Whipple, K.X., Burchfield, B.C., Zhang, X., Tang, W., 2005. Late Cenozoic uplift of southeastern Tibet. Geology 33, 525–528.

Clauzon, G., Suc, J.-P., Gautier, F., Berger, A., Loutre, M.-F., 1996. Alternate interpretation of the Messinian salinity crisis: controversy resolved? Geology 24, 363–366.

Cosentino, D., Gliozzi, E., 1988. Considerazioni sulle velocità di sollevamento di depositi eutirreniani dell'Italia meridionale e della Sicilia. Mem. Soc. Geol. Ital. 42, 653–665.

Cosentino, D., Cipollari, P., Di Bella, L., Esposito, A., Faranda, C., Giordano, G., Gliozzi, E.,Mattei,M., Mazzini, I., Porreca, M., Funiciello, R., 2009. Tectonics, sea-level changes and palaeoenvironments in the early Pleistocene of Rome (Italy). Quat. Res. 72, 143–155.

Cosentino, D., Radeff, G., Darbas, G., Dudas, F.O., Gurbuz, K., Schildgen, T.F., 2010. Late Miocene geohistory of the Mut and Adana basins (southern Turkey): insight for uplift of the southern margin of the Central Anatolian Plateau. Tectonic Crossroads: Evolving orogens of Eurasia–Africa–Arabia, Middle East Technical University, Ankara, Turkey, pp. 4–8 (October, 2010).

Cosentino, D., Schildgen, T.F., Cipollari, P., Faranda, C., Gliozzi, E., Hudácková, N., Lucifora, S., Strecker, M.R., in press. Late Miocene surface uplift of the southern margin of the Central Anatolian plateau, Central Taurides, Turkey. Geol. Soc. Am. Bull., doi:10.1130/B30466.1 (Electronic publication ahead of print October 21, 2011).

Crosby, B.T., Whipple, K.X., 2006. Knickpoint initiation and distribution within fluvial networks: 236 waterfalls in the Waipaoa River, North Island, New Zealand. Geomorphology 82, 16–38.

Dethier, D.P., Pessl, F., Keuler, R.F., Balzarini, M.A., Pevear, D.R., 1995. Late Wisconsinan glaciomarine deposition and isostatic rebound, northern Puget lowland, Washington. Geol. Soc. Am. Bull. 107, 1288–1303.

Dewey, J.F., Sengör, A.M.C., 1979. Aegean and surrounding regions: complex multiplate and continuum tectonics in a convergent zone. Geol. Soc. Am. Bull. 90, 84–92.

Duretz, T., Gerya, T.V., May, D.A., 2011. Numerical modelling of spontaneous slab breakoff and subsequent topographic response. Tectonophysics 502, 244–256.

Duvall, A., Kirby, E., Burbank, D., 2004. Tectonic and lithologic controls on bedrock channel profiles and processes in coastal California. J. Geophys. Res. 109, F03002. doi:10.1029/2003jf000086.

Faccenna, C., Becker, T.W., 2011. Shaping mobile belts by small-scale convection. Nature 465 (7298), 602–605.

Faccenna, C., Bellier, O., Martinod, J., Piromallo, C., Regard, V., 2006. Slab detachment beneath eastern Anatolia: a possible cause for the formation of the North Anatolian fault. Earth Planet. Sci. Lett. 242, 85–97.

Flint, J.J., 1974. Stream gradient as a function of order, magnitude, and discharge. Water Resour. Res. 10, 969–973.

Fuller, I.C., Macklin, M.G., Lewin, J., Passmore, D.G., Wintle, A.G., 1998. River response to high-frequency climate oscillations in southern Europe over the past 200 k.y. Geology 26, 275–278.

Gans, C.R., Beck, S.L., Zandt, G., Biryol, C.B., Ozacar, A.A., 2009. Detecting the limit of slab break-off in central Turkey: new high-resolution Pn tomography results. Geophys. J. Int. 179, 1566–1577.

Gardner, T.W., Verdonck, D., Pinter, N.M., Slingerland, R., Furlong, K.P., Bullard, T.F., Wells, S.G., 1992. Quaternary uplift astride the aseismic Cocos Ridge, Pacific coast, Costa Rica. Geol. Soc. Am. Bull. 104, 219–232.

Gardosh, M.A., Druckman, Y., 2006. Seismic stratigraphy, structure, and tectonic evolution of the Levantine basin, offshore Israel. In: Robertson, A.H.F., Mountrakis, D. (Eds.), Tectonic Development of the Eastern Mediterranean Region: Geol. Soc., Lond., Spec. Publ., 260, pp. 201–227.

Gile, L.H., Peterson, F.F., Grossman, R.B., 1966. Morphological and genetic sequences of carbonate accumulation in desert soils. Soil Sci. 101, 347–360.
Goethals, M.M., Hetzel, R., Niedermann, S., Wittmann, H., Fenton, C.R., Kubik, P.W., Christl, M., von Blanckenburg, F., 2009. An improved experimental determination of cosmogenic 10Be/21Ne and 26Al/21Ne production ratios in quartz. Earth Planet. Sci. Lett. 284, 187–198.
Gögüs, O.H., Pysklywec, R.N., 2008. Mantle lithosphere delamination driving plateau uplift and synconvergent extension in eastern Anatolia. Geology 36, 723–726.
Gök, R., Sandvol, E., Turkelli, N., Seber, D., Barazangi, M., 2003. Sn attenuation in the Anatolian and Iranian plateau and surrounding regions. Geophys. Res. Lett. 30, 8042.
Gök, R., Pasyanos, M.E., Zor, E., 2007. Lithospheric structure of the continent–continent collision zone: eastern Turkey. Geophys. J. Int. 169, 1079–1088.
Gosse, J.C., Phillips, F.M., 2001. Terrestrial in-situ cosmogenic nuclides: theory and application. Quat. Sci. Rev. 20, 1475–1560.
Govers, R., 2009. Choking the Mediterranean to dehydration: the Messinian salinity crisis. Geology 37 (2), 167–170.
Gubbels, T.L., Isacks, B.L., Farrar, E., 1993. High-level surfaces, plateau uplift, and foreland development, Bolivian Central Andes. Geology 21, 695–698.
Hancock, G.S., Anderson, R.S., 2002. Numerical modeling of fluvial strath-terrace formation in response to oscillating climate. Geol. Soc. Am. Bull. 114, 1131–1142.
Harkins, N., Kirby, E., Heimsath, A., Robinson, R., Reiser, U., 2007. Transient fluvial incision in the headwaters of the Yellow River, notheastern Tibet, China. J. Geophys. Res. 112 (F3), F03S04. doi:10.1029/2006jf000570.
Harrison, R., Newell, W., Panayides, I., Stone, B., Tsiolakis, E., Necdet, M., Batihanli, H., Ozhur, A., Lord, A., Berksoy, O., Zomeni, Z., Schindler, J.S., 2008. Bedrock geologic map of the Greater Lefkosia area, Cyprus, Scientific Investigations Map 3046, 1 map, scale 1:25,000, 36-p. text.
Hilley, G.E., Arrowsmith, J.R., 2008. Geomorphic response to uplift along the Dragon's Back pressure ridge, Carrizo Plain, California. Geology 36, 367–370.
Hoke, G.D., Isacks, B.L., Jordan, T.E., Blanco, N., Tomlinson, A.J., Ramezani, J., 2007. Geomorphic evidence for post-10 Ma uplift of the western flank of the central Andes 18 degrees 30"-22 degrees S. Tectonics 26, TC5021. doi:10.1029/2006tc002082.
Hüsing, S.K., Zachariasse, W.-J., van Hinsbergen, D.J.J., Krijgsman, W., Inceöz, M., Harzhauser, M., Mandic, O., Kroh, A., 2009. Oligocene Miocene basin evolution in SE Anatolia, Turkey: constraints on the closure of the eastern Tethys gateway. In: van Hinsbergen, D.J.J., Edwards, M.A., Govers, R. (Eds.), Collision and Collapse at the Africa–Arabia–Eurasia Subduction Zone: Geol. Soc., Lond., Spec. Publ., 311, pp. 107–132.
Iaccarino, S.M., Premoli, S.I., Biolz, M., Foresi, L.M., Lirer, F., Urco, E., Petrizzo, M.R., 2007. Practical manual of Neogene planktonic foraminifera. International School on Planktonic Foraminifera. VI Course. Neogene, Perugia (Italy), pp. 1–181. Feb. 19–23, 2007.
Jaffey, N., Robertson, A., 2005. Non-marine sedimentation associated with Oligocene–Recent exhumation and uplift of the Central Taurus Mountains, S Turkey. Sediment. Geol. 173, 53–89.
Jarvis, A., Reuter, H.I., Nelson, A., Guevara, E., 2008. Hole-filled SRTM for the globe Version 4, available from the CGIAR-CSI SRTM 90m Database. http://srtm.csi.cgiar. org2008.
Jordan, T.E., Nester, P.L., Blanco, N., Hoke, G.D., Davila, F., Tomlinson, A.J., 2010. Uplift of the Altiplano–Puna plateau: a view from the west. Tectonics 29, TC5007. doi:10.1029/2010tc002661.
Kelling, G., Gökçen, S.L., Floyd, P.A., Gökçen, N., 1987. Neogene tectonics and plate convergence
in the eastern Mediterranean: new data from southern Turkey. Geology 15, 425–429.
Keskin, M., 2003. Magma generation by slab steepening and breakoff beneath a subduction accretion complex: an alternative model for collision-related volcanism in Eastern Anatolia, Turkey. Geophys. Res. Lett. 30 (24), 8046. doi:10.1029/2003GL018019.
Kinnaird, C., Robertson, A.H.F., Morris, A., 2011. Timing of uplift of the Troodos massif (Cyprus) constrained by sedimentary and magnetic polarity evidence. J. Geol. Soc. 168, 457–470. doi:10.1144/0016-76492009-150.
Kirby, E., Whipple, K.X., 2001. Quantifying differential rock-uplift rates via stream profile analysis. Geology 29, 415–418.
Kirby, E., Whipple, K.X., Tang, W., Chen, Z., 2003. Distribution of active rock uplift along the eastern margin of the Tibetan Plateau: inferences from bedrock channel longitudinal profiles. J. Geophys. Res. 108, 2217. doi:10.1029/2001JB000861.
Korschinek, G., Bergmaier, A., Faestermann, T., et al., 2010. A new value for the half-life of 10Be by heavy-ion elastic recoil detection and liquid scintillation counting. Nuclear Instruments and Methods in Physics Research Section B — Beam Interactions with Materials and Atoms 268 (2), 187–191.
Krijgsman, W., Hilgen, F.J., Raffi, I., Sierro, F.J., Wilson, D.S., 1999. Chronology, causes and progression of the Messinian salinity crisis. Nature 400, 652–655.

Lague, D., Davy, P., 2003. Constraints on the long-term colluvial erosion law by analyzing slope–area relationships at various tectonic uplift rates in the Siwaliks Hills (Nepal). J. Geophys. Res. 108, 2129. doi:10.1029/2002jb001893.

Lal, D., 1991. Cosmic ray labeling of erosion surfaces: in-situ nuclide production rates and erosion models. Earth Planet. Sci. Lett. 104, 424–439.

Lavé, J., Avouac, J.P., 2001. Fluvial incision and tectonic uplift across the Himalayas of central Nepal. J. Geophys. Res. 106 (B11), 26,561–26,591.

Lei, J., Zhao, D., 2007. Teleseismic evidence for a break-off subducting slab under Eastern Turkey. Earth Planet. Sci. Lett. 257, 14–28.

Lisiecki, L.E., Raymo, M.E., 2005. A Pliocene–Pleistocene stack of 57 globally distributed benthic %18O records. Paleoceanography 20, PA1003. doi:10.1029/2004PA001071.

Lourens, L., Hilgen, F., Shackleton, N.J., Laskar, J., Wilson, J., 2004. Appendix 2. Orbital tuning calibrations and conversions for the Neogene Period. In: Gradstein, F.M., Ogg, J.G., Smith, A.G. (Eds.), A Geologic Time Scale 2004. Cambridge University Press, Cambridge UK, pp. 469–471.

Makris, J., Ben-Avraham, Z., Behle, A., Ginzburg, A., Giese, P., Steinmetz, L., Whitmarsh, R.B., Eleftheriou, S., 1983. Seismic refraction profiles between Cyprus and Israel and their interpretation. Geophys. J. R. Astron. Soc. 75, 575–591.

Melnick, D., Bookhagen, B., Strecker, M.R., Echtler, H.P., 2009. Segmentation of megathrust rupture zones from fore-arc deformation patterns over hundreds to millions of years, Arauco Peninsula, Chile. J. Geophys. Res. 114, B01407. doi:10.1029/2008jb005788.

Merritts, D., Bull, W.B., 1989. Interpreting Quaternary uplift rates at the Mendocino Triple Junction, northern California, from uplifted marine terraces. Geology 17, 1020–1024.

Merritts, D., Vincent, K., Wohl, E.T., 1994. Long river profiles, tectonism, and eustasy: a guide to interpreting fluvial terraces. J. Geophys. Res. 99 (B7), 14031–14050.

Meyer, G.A., Wells, S.G., Jull, A.J.T., 1995. Fire and alluvial chronology in Yellowstone National Park: climate and intrinsic controls on Holocene geomorphic processes. Geol. Soc. Am. Bull. 107, 1211–1230.

Molin, P., Pazzaglia, F.J., Dramis, F., 2004. Geomorphic expression of active tectonics in a rapidly-deforming forearc, Sila Massif, Calabria, southern Italy. Am. J. Sci. 304, 559–589.

Niemann, J.D., Gasparini, N.M., Tucker, G.E., Bras, R.L., 2001. A quantitative evaluation of Playfair's law and its use in testing long-term stream erosion models. Earth Surf. Process. Landforms 26, 1317–1332.

Nishiizumi, K., Lal, D., Klein, J., Middleton, R., Arnold, J.R., 1986. Production of 10Be and 26Al by cosmic rays in terrestrial quartz in situ and implications for erosion rates. Nature 319, 134–136.

Nishiizumi, K., Imamura, M., Caffee, M.W., Southon, J.R., Finkel, R.C., McAninch, J., 2007. Absolute calibration of 10Be AMS standards. Nucl. Instrum. Methods Phys. Res., Sect. B 258, 403–413.

Pan, B.T., Burbank, D., Wang, Y.X., Wu, G.J., Li, J.J., Guan, Q.Y., 2003. A 900 ky record of strath terrace formation during glacial–interglacial transitions in northwest China. Geology 31, 957–960.

Pazzaglia, F.J., Brandon, M.T., 2001. A fluvial record of long-term steady-state uplift and erosion across the Cascadia Forearc High, western Washington State. Am. J. Sci. 301, 385–431.

Pazzaglia, F.J., Gardner, T.W., 1993. Fluvial terraces of the lower Susquehanna River. Geomorphology 8, 83–113.

Pearce, J.A., Bender, J.F., Delong, S.E., Kidd, W.S.F., Low, P.J., Guner, Y., Saroglu, F., Yilmaz, Y., Moorbath, S., Mitchell, J.G., 1990. Genesis of collision volcanism in Eastern Anatolia, Turkey. J. Volcanol. Geotherm. Res. 44, 189–229.

Perg, L.A., Anderson, R.S., Finkel, R.C., 2001. Use of a new 10Be and 26Al inventory method to date marine terraces, Santa Cruz, California, USA. Geology 29, 879–882.

Pourteau, A., Candan, O., Oberhänsli, R., 2010. High-pressure metasediments in central Turkey: constraints on the Neotethyan closure history. Tectonics 29, TC5004. doi:10.1029/2009TC002650.

Quade, J., Garzione, C., Eiler, J., 2007. Paleoelevation reconstruction using pedogenic carbonates. Rev. Mineral. Geochem. 66, 53–87.

Raf", I., 2002. Revision of the early–middle Pleistocene calcareous nannofossil biochronology (1.75–0.85 Ma). Mar. Micropaleontol. 45, 25–55.

Repka, J.L., Anderson, R.S., Finkel, R.C., 1997. Cosmogenic dating of fluvial terraces, Fremont River, Utah. Earth Planet. Sci. Lett. 152, 59–73.

Riihimaki, C., Libarkin, J., 2007. Terrestrial cosmogenic nuclides as paleoaltimetric proxies. Rev. Mineral. Geochem. 66, 269–278.

Robertson, A.H.F., 1998. Tectonic significance of the Eratosthenes Seamount: a continental fragment in the process of collision with a subduction zone in the eastern Mediterranean (Ocean Drilling Program Leg 160). Tectonophysics 298, 63–82.

Robertson, A.H.F., 2000. Mesozoic–Tertiary tectonic–sedimentary evolution of a south Tethyan basin and its margins in southern Turkey. In: Bozkurt, E., Winchester, J.A., Piper, J.D.A. (Eds.), Tectonics and Magmatism in Turkey and the Surrounding Area: Geol. Soc., Lond., Spec. Publ., 173, pp. 97–138.

Robertson, A.H.F., Dixon, J.E., Brown, S., Collins, S., Pickett, E., Sharp, I., Ustafmer, T., 1996. Alternative tectonic models for the Late Palaeozoic–Early Tertiary development of Tethys in the Eastern Mediterranean region. In: Morris, A., Tarling, D.H. (Eds.), Palaeomagnetism and Tectonics of the Mediterranean Region: Geol. Soc., Lond., Spec. Publ., 105, pp. 239–263.

Robertson, A.H.F., Parlak, O., Ustaömer, T., 2009. Melange and ophiolite emplacement related to subduction of the northern margin of the Tauride–Anatolide continent, central and western Turkey. In: Van Hinsbergen, D.J.J., Edwards, M.A., Govers, R. (Eds.), Collision and Collapse at the Africa–Arabia–Eurasia Subduction Zone: Geol. Soc., Lond., Spec. Publ., 311, pp. 9–66.

Rosenbloom, N.A., Anderson, R.S., 1994. Evolution of the marine terraced landscape, Santa Cruz, California. J. Geophys. Res. 99, 14,013–14,030.

Sahagian, D., Proussevitch, A., 2007. Paleoelevation measurement on the basis of vesicular basalts. Rev. Mineral. Geochem. 66, 195–213.

Schattner, U., 2010. What triggered the early-to-mid Pleistocene tectonic transition across the entire eastern Mediterranean? Earth Planet. Sci. Lett. 289, 539–548.

Schildgen, T., Dethier, D.P., Bierman, P., Caffee, M., 2002. Al-26 and Be-10 dating of late Pleistocene and Holocene fill terraces: a record of fluvial deposition and incision, Colorado Front Range. Earth Surf. Process. Landforms 27 (7), 773–787.

Schildgen, T.F., Phillips, W.M., Purvis, R.S., 2005. Simulation of snow shielding corrections for cosmogenic nuclide surface exposure studies. Geomorphology 64, 67–85.

Schildgen, T.F., Hodges, K.V., Whipple, K.X., Reiners, P.W., Pringle, M.S., 2007. Uplift of the western margin of the Andean plateau revealed from canyon incision history, southern Peru. Geology 35, 523–526.

Schildgen, T.F., Hodges, K.V., Whipple, K.X., Pringle, M.S., van Soest, M., Cornell, K., 2009a. Late Cenozoic structural and tectonic development of the western margin of the Central Andean Plateau in southwest Peru. Tectonics 28, TC4007. doi:10.1029/2008tc002403.

Schildgen, T.F., Ehlers, T.A., Whipp, D.M., van Soest, M.C., Whipple, K.X., Hodges, K.V., 2009b. Quantifying canyon incision and Andean Plateau surface uplift, southwest Peru: a thermochronometer and numerical modelling approach. J. Geophys. Res. 114, F04014. doi:10.1029/2009jf001305.

Seeber, L., Gornitz, V., 1983. River profiles along the Himalayan Arc as indicators of active tectonics. Tectonophysics 92, 335–367.

Senel, M., 2002. Geological Map of Turkey, Konya (No. 14): Maden Tetkik ve Arama Genel Müdürlügü (MTA), M. Senel, (Ed.) scale 1;500,000, 1 sheet.

Sengör, A.M.C., Yılmaz, Y., 1981. Tethyan evolution of Turkey: a plate tectonic approach. Tectonophysics 75, 181–241.

Sengör, A.M.C., Yılmaz, Y., Süngürlu, O., 1984. Tectonics of the Mediterranean Cimmerides: nature and evolution of the western termination of Palaeo-Tethys. In: Dixon, J.E., Robertson, A.H.F. (Eds.), The Geological Evolution of the Eastern Mediterranean: Geol: Soc., Lond., Spec. Publ., 17, pp. 77–112.

Sengör, A.M.C., Görür, N., Saroglu, F., 1985. Strike-slip faulting and basin related formation in zones of tectonic escape. Soc. Econ. Paleontol. Mineral. Spec. Publ. 37, 227–440.

Sengör, A.M.C., Ozeren, S., Genç, T., Zor, E., 2003. East Anatolian high plateau as a mantle-supported, north–south shortened domal structure. Geophys. Res. Lett. 30, 8045. doi:10.1029/2003GL017858.

Seyrek, A., Demir, T., Pringle, M., Yurtman, S., Westaway, R., Bridgland, D., Beck, A., Rowbotham, G., 2008. Late Cenozoic uplift of the Amanos Mountains and incision of the Middle Ceyhan river gorge, southern Turkey; Ar–Ar dating of the Düziçi basalt. Geomorphology 97, 321–355.

Snyder, N.P., Whipple, K.X., Tucker, G.E., Merritts, D.M., 2000. Landscape response to tectonic forcing: digital elevation model analysis of stream profiles in the Mendocino triple junction region, northern California. Geol. Soc. Am. Bull. 112, 1250–1263.

Stone, J.O., 2000. Air pressure and cosmogenic isotope production. J. Geophys. Res. 105, 23,753–23,759.

Tanar, U., Gökçen, N., 1990. Mut–Ermenek Tersiyer istifinin stratigrafisi ve mikropaleontolojisi. Maden Tetkik ve Arama Genel Müdürlügü (MTA) Dergisi, 110, pp. 175–180.

Tucker, G.E., Slingerland, R., 1997. Drainage basin response to climate change. Water Resour. Res. 33, 2031–2047.

Ulu, Ü., 2002. Geological map of Turkey, Adana (No. 15): Maden Tetkik ve Arama Genel Müdürlügü (MTA), ed. M. Senel, scale 1;500,000, 1 sheet.

van Hunan, J., Allen, M.B., 2011. Continental collision and slab break-off: a comparison of 3-D numerical models with observations. Earth Planet. Sci. Lett. 302, 27–37.

Wegmann, K.W., Pazzaglia, F.J., 2002. Holocene strath terraces, climate change, and active tectonics; the Clearwater River basin, Olympic Peninsula, Washington State. Geol. Soc. Am. Bull. 114, 731–744.

Wegmann, K.W., Pazzaglia, F.J., 2009. Late Quaternary fluvial terraces of the Romagna and Marche Apennines, Italy: climatic, lithologic, and tectonic controls on terrace genesis in an active orogen. Quat. Sci. Rev. 28, 137–165.

Westaway, R., 1993. Quaternary uplift of southern Italy. J. Geophys. Res. 98 (B12), 21741–21772.

Westaway, R., Pringle, M., Yurtmen, S., Demir, T., Bridgland, D., Rowbotham, G., Maddy, D., 2004. Pliocene and Quaternary regional uplift in western Turkey: the Gediz River terrace staircase and the volcanism at Kula. Tectonophysics 391, 121–169.

Whipple, K.X., 2001. Fluvial landscape response time: how plausible is steady-state denudation? Am. J. Sci. 301, 313–325.

Whipple, K.X., 2004. Bedrock rivers and the geomorphology of active orogens. Annu. Rev. Earth Planet. Sci. 32, 151–185.

Whipple, K.X., Tucker, G.E., 1999. Dynamics of the stream-power river incision model: Implications for height limits of mountain ranges, landscape response timescales, and research needs. J. Geophys. Res. 104, 17,661–17,674.

Williams, G.D., Ünlügenç, U.C., Kelling, G., Demirkol, C., 1995. Tectonic controls on stratigraphical evolution of the Adana basin. J. Geol. Soc. 152, 873–882.

Wobus, C.W., Whipple, K.X., Kirby, E., Snyder, N., Johnson, J., Spyropolou, K., Crosby, B., Sheehan, D., 2006. Tectonics from topography: Procedures, promise, and pitfalls. In: Willett, S.D., et al. (Ed.), Tectonics, Climate, and Landscape Evolution: Geol. Soc. Am. Spec. Pap., 398, pp. 55–74.

Woodside, J.M., 1977. Tectonic elements and crust of the eastern Mediterranean Sea. Mar. Geophys. Res. 3, 317–354.

Yıldırım, C., Schildgen, T.F., Echtler, H., Melnick, D., Strecker, M.R., 2011. Late Neogene orogenic uplift in the Central Pontides associated with the North Anatolian Fault — implications for the northern margin of the Central Anatolian Plateau, Turkey. Tectonics 30, TC5005. doi:10.1029/2010TC002756.

Yıldız, A., Toker, V., Demircan, H., Sevim, S., 2003. Paleoenvironmental interpretation and findings of Pliocene–Pleistocene nannoplankton, planktic foraminifera, trace fossil in the Mut Basin. Yerbilimleri 28, 123–144.

Yılmaz, Y., Tüysüz, O., Yigitbas, E., Genç, S.C., Sengör, A.M.C., 1997. Geology and tectonic evolution of the Pontides. In: Robinson, A.G. (Ed.), Regional and Petroleum Geology of the Black Sea and Surrounding Region: Am. Assoc. Petroleum Geologists Memoir, Tulsa, OK, 68, pp. 183–266.

York, D., 1969. Least squares fitting of a straight line with correlated errors. Earth Planet. Sci. Lett. 5, 320–324.

Zazo, C., Goy, J.L., Dabrio, C.J., Bardaji, T., Hillaire-Marcel, C., Ghaleb, B., Gonzalez-Delgado, J.A., Soler, V., 2003. Pleistocene raised marine terraces of the Spanish Mediterranean and Atlantic coasts: records of coastal uplift, sea-level highstands and climate changes. Mar. Geol. 194, 103–133.

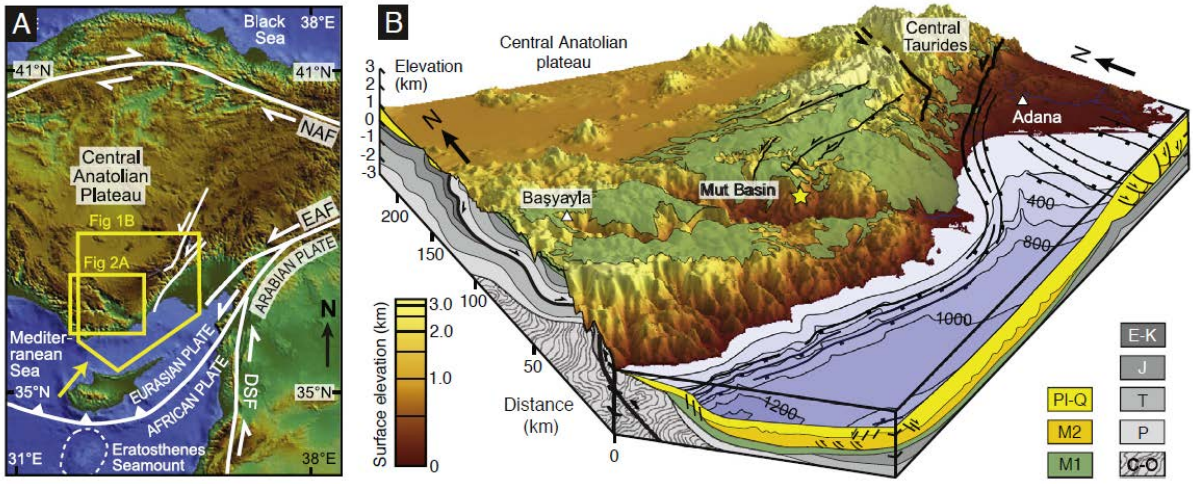

Fig. 1. A: Regional simplified tectonic and topographic map and B: perspective view of topography across the Central Anatolian plateau and its southern margin with 7:1 vertical exaggeration, modified from Cosentino et al. (in press). Yellow pentagon in A indicates edges of the three-dimensional perspective topography in B, and yellow rectangle outlines map in Fig. 2A. Low topography within the yellow rectangle is the modern Mut Basin. NAF: North Anatolian Fault; EAF: East Anatolian Fault; DSF: Dead Sea Fault. In B, surface colors indicate elevation, except for the green overlay, which indicates the outcrop pattern of Late Miocene marine sediments; outcrop pattern and bedrock cross-section interpreted from 1:500,000 geology maps (Senel, 2002; Ulu, 2002). Offshore cross-section and 200-m bathymetric contours based on Aksu et al. (2005). Yellow star indicates Calabrian (Early Pleistocene) marine section (Yıldız et al., 2003). C-O: Cambro-Orodivician; P: Permian; T: Triassic; J: Jurassic; E-K: Eocene to Cretaceous; M1: Miocene (pre-Messinian); M2: Miocene (Messinian); Pl-Q: Plio-Quaternary. (For interpretation of the references to color in this figure legend, the reader is referred to the web version of this article.)

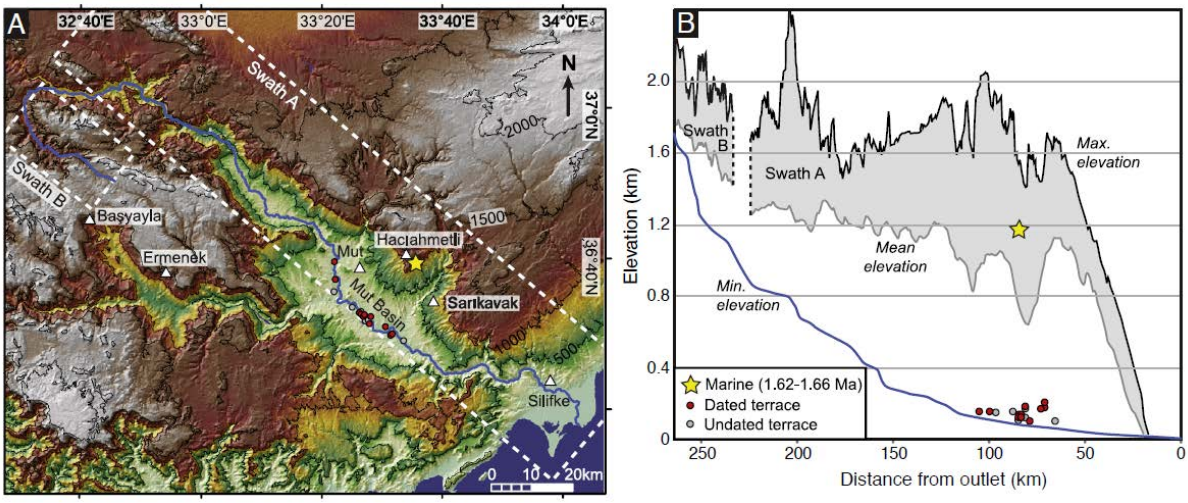

Fig. 2. A: Map of the Mut Basin, showing the main branch of the Göksu River (light blue) and positions of fluvial terraces and uplifted Pleistocene marine sediments. Topography from 90-m resolution SRTM data (Jarvis et al., 2008) with 500 m contour intervals. B: River profile along the Göksu River, with projected positions of terraces and Pleistocene marine sediments. Gray and black lines (with area shaded between) indicate mean and maximum elevation values from the swath profiles shown in A. (For interpretation of the references to color in this figure legend, the reader is referred to the web version of this article.)

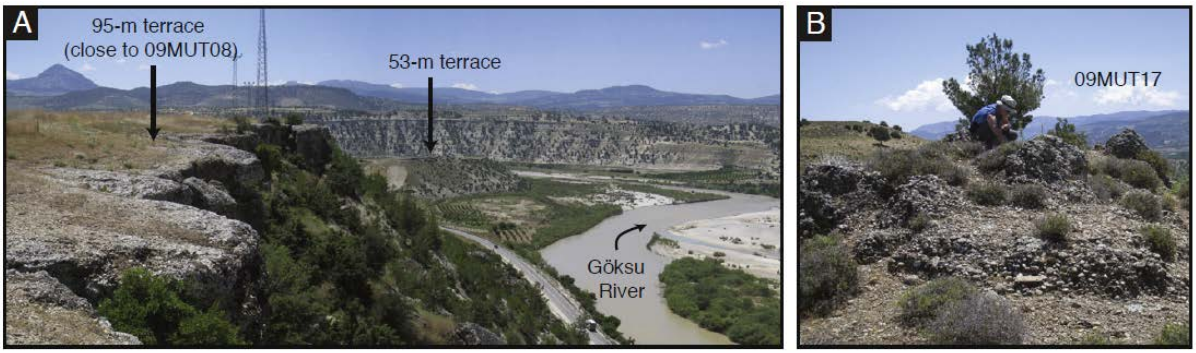

Fig. 3. Gravel-capped fluvial strath terraces of the Mut Basin. A: Intermediate height terraces showing cemented, flat top surfaces with thin cap of fine-grained (overbank) material. B: Degraded surface of the 110-m terrace of sample 09MUT17.

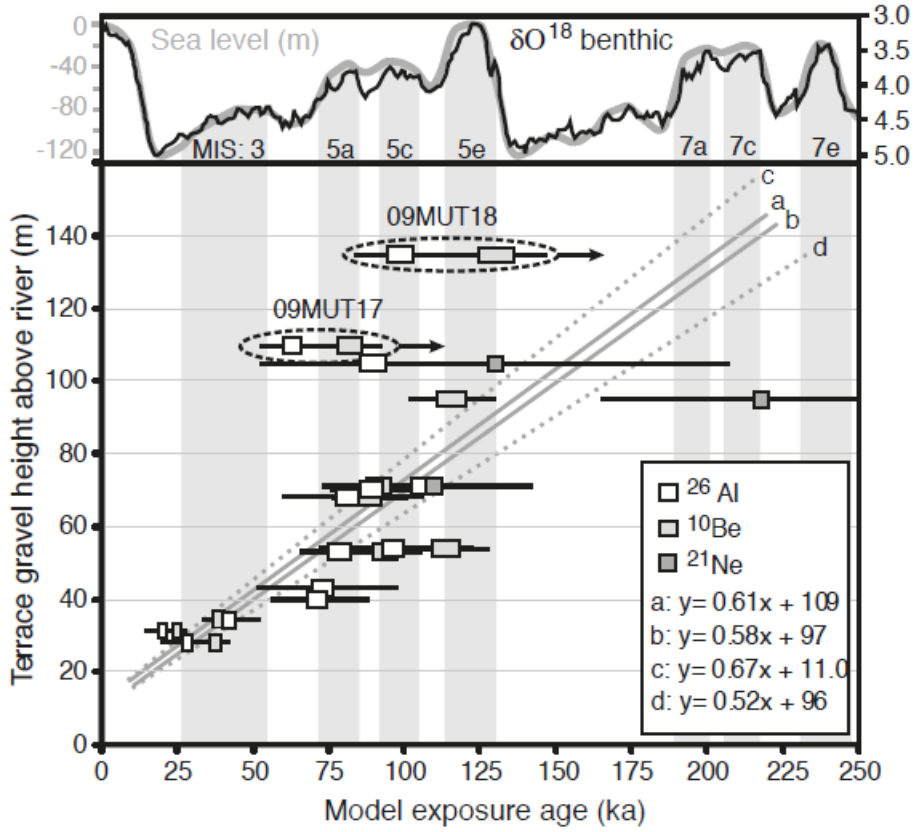

Fig. 4. Exposure ages for fluvial strath terraces of the Mut Basin. For ^{10}Be and ^{26}Al, boxes represent range of mean ages calculated using different scaling schemes (see Table A2). Bars on symbols show full range of 2σ errors. Y-axis errors are smaller than the symbol. Sea level variations from Bintanja et al. (2005) and δO18 data from Lisiecki and Raymo (2005). Odd-numbered marine isotope stages (MIS) are highlighted with gray shading. Ages of circled samples (09MUT17 and 09MUT18) are interpreted as minimum ages (see text for explanation). Two solid gray lines show York (1969) regression fits to all data except the old ^{21}Ne outlier and the two terraces with minimum ages, with (a) using the maximum calculated ages, and (b) using the minimum calculated ages (see Tables A2 and A4). Dotted gray lines (c and d) outline the range of fits acceptable within a 95% confidence interval for both maximum and minimum calculated ages.

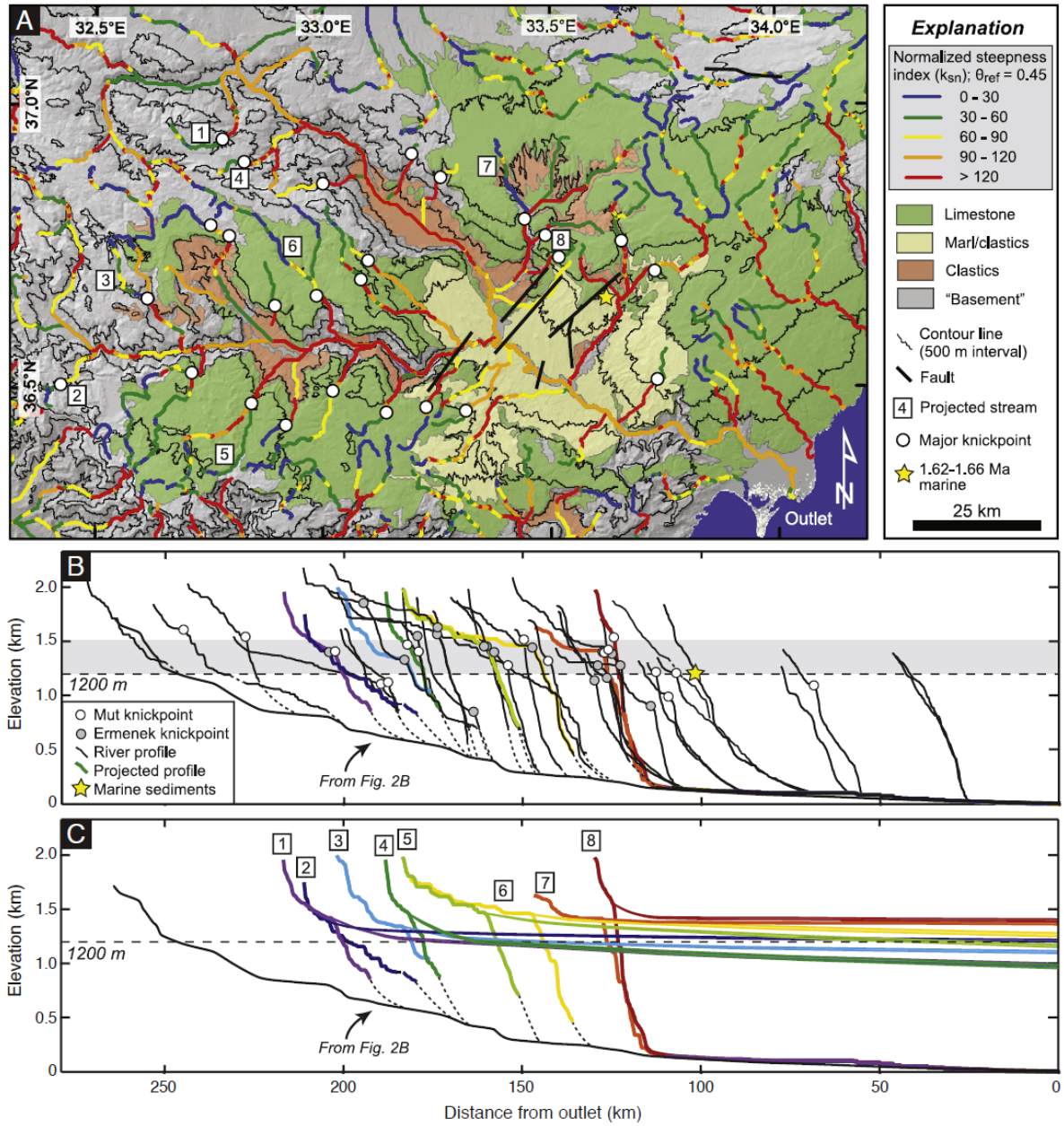

Fig. 5. A: Map of channel steepness indexes that are normalized (k_{sn}) to a reference concavity (θ_{ref}) of 0.45 throughout the Mut and Ermenek basins, calculated using the stream profiler tool (www.geomorphtools.org) with a smoothing window of 500 m. Geology from 1:500,000 scale maps (Senel, 2002; Ulu, 2002). Channels with numbered labels were used for projections. B: Longitudinal channel profiles with major knickpoints marked by circles. Knickpoints colored based on their position in the Mut or Ermenek sub-basin. C: Channel projections of upper, relict portions of channels to the position of the modern outlet. Ranges of final projected heights reflect 2σ errors in k_s and a best-fit concavity value based on log (slope) versus log (area) plots of the upper channel segment.

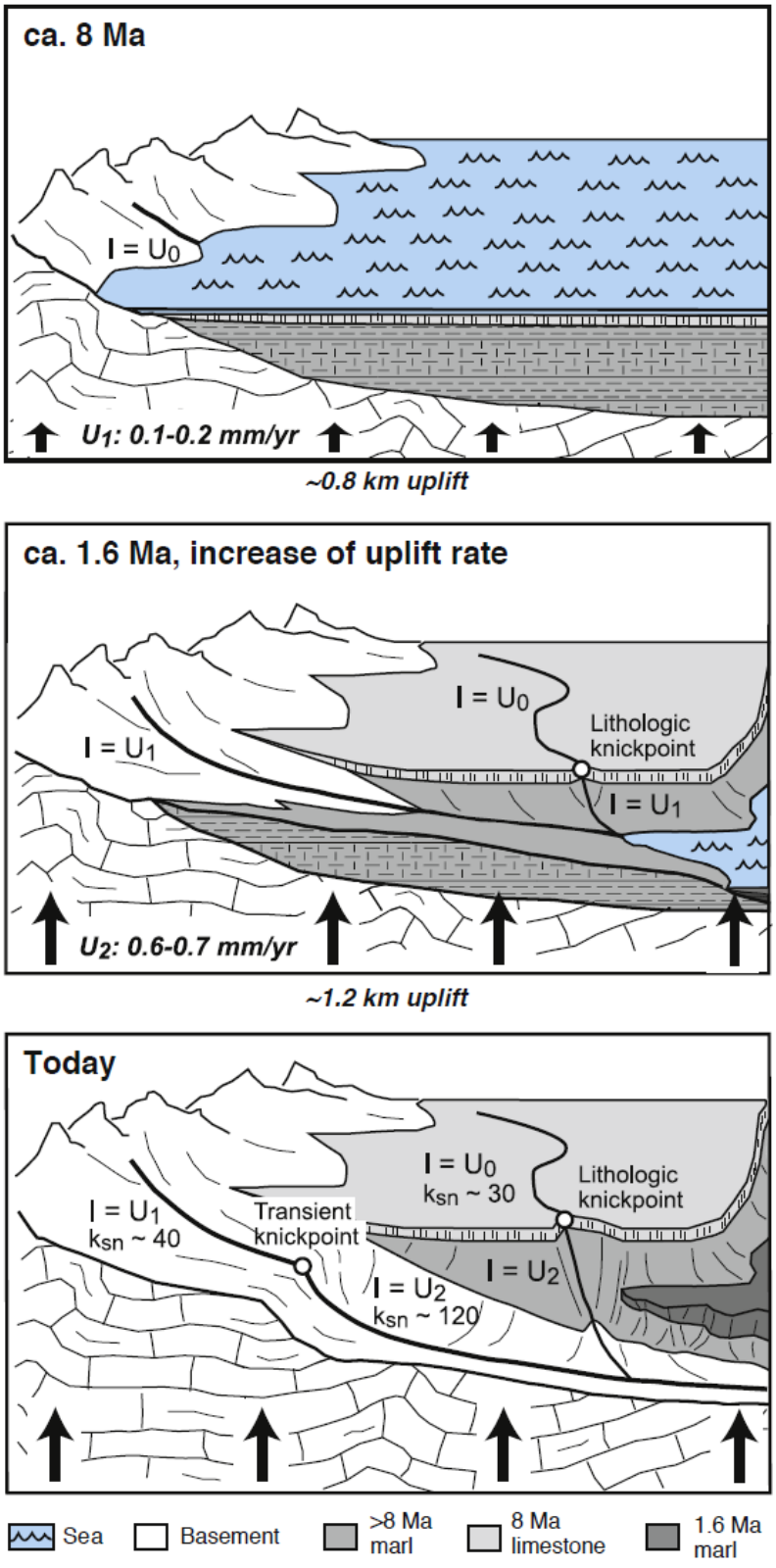

Fig. 6. Schematic evolution of the southernmargin of the Central Anatolian plateau, illustrating initial uplift of ca. 8Mamarine sediments to an elevation of ca. 0.8 km followed by deposition of Pliocene–Pleistocene marine sediments, and an additional ca. 1.2 km of rapid uplift that continues to today. Channels within the basement respond to changing uplift rates, while channels in the Mut Formation (8Ma limestones) are predominantly controlled by the lithologic contact. U: uplift rate; I: incision rate; k_{sn}: normalized steepness index.

Table 1
Initial uplift rates derived from channel projections*.

Channel #	Concavity	k_s	k_s error	ΔZ high[a]	ΔZ high[b]	U_i high[c]	U_i low[d]
			(2σ)	(m)	(m)	(mm yr^{-1})	(mm yr^{-1})
Channels incising basement							
1	0.51	121	3	972	993	0.14	0.13
2	0.60	308	6	1189	1197	0.01	0.00
3	0.70	4655	214	1087	1109	0.07	0.06
4	0.51	46	4	950	982	0.15	0.13
Channels incising Mut Formation							
5	0.42	19.6	0.8	1145	1170	0.03	0.02
6	0.50	86	8	1246	1280	−0.03	−0.05
7	0.80	17	4	1353	1356	−0.09	−0.10
8	0.67	966	44	1393	1408	−0.12	−0.13

* Assumes $U_f = 0.74$ mm yr^{-1} and $\Delta t = 1.63$ Ma.
[a] From $k_s - 2\sigma$ value
[b] From $k_s + 2\sigma$ value
[c] Using low estimate for ΔZ
[d] Using high estimate for ΔZ

Appendix

Supplementary Material

Sample preparation and analysis for cosmic nuclides

Surface ages of sampled strath terraces were determined using standard analytical procedures from concentrations of in-situ produced ^{10}Be, ^{26}Al, and ^{21}Ne in chert from capping alluvial gravels. We have streamlined previous processing methods (e.g., Kohl and Nishiizumi, 1992; von Blanckenburg et al., 2004). An updated, step-by-step manual is available at http://www.geog.ucsb.edu/~bodo/pdf/ bookhagen_chemSeparation_UCSB.pdf. In short, after crushing the chert clasts, we cleaned the 0.25-1.0 mm size fraction first through a 12-hour bath in a 1:1 hydrochloric acid and water solution. Next, samples were leached at least four times in a 2% hydrofluoric acid solution in an ultrasonic bath to remove meteoric beryllium. Our cleaned samples were between ~40 and ~60 g. Because more than 50% of material was dissolved in each cleaning step, several samples ("undated terraces" of Fig. 2) yielded insufficient amounts of clean material for analysis. Approximately 3 g of the cleaned material were reserved for ^{21}Ne analysis, and the remainder of material was processed to isolate ^{10}Be and ^{26}Al. Samples were dissolved in hydrofluoric acid, and after addition of a low-ratio ^{9}Be carrier (^{10}Be/^{9}Be ratio of ~$1x10^{-15}$), Be and Al were separated by ion-exchange chromatography. Stable ^{27}Al concentrations were determined by ICP-OES (Varian 720 ES) at GFZ Potsdam using mainly the 167.019 nm wavelength.

For cosmogenic ^{21}Ne determination at GFZ Potsdam, samples were wrapped in Al foil and loaded in the sample carrousel above the extraction furnace, which was then baked at 100°C for about one week. The noble gases were extracted by stepwise heating (at 400, 600, 800, and 1200°C) for at least 20 minutes each. In addition, aliquots of 08TSERM04 and 09MUT12 were crushed in vacuo to determine the isotopic composition of the trapped (non-cosmogenic) Ne component. In each case, after gas extraction chemically active gases were removed in two Ti sponges and two SAES (ZrAl) getters, and He, Ne, and Ar-Kr-Xe were separated from each other by trapping in a cryogenic adsorber and subsequent sequential release. Noble gas concentrations and isotopic compositions were determined in a VG5400 sector field mass spectrometer, and were corrected for isobaric interferences, instrumental mass fractionation, and analytical blanks. Further details about the analytical procedures can be found in Niedermann et al. (1997).

The two crushing extractions yielded ^{21}Ne/^{20}Ne ratios consistent with the atmospheric value 0.002959 (Table A3); therefore, all ^{21}Ne excesses were calculated relative to atmospheric composition. In most heating steps, the ^{21}Ne/^{20}Ne ratios are only moderately increased; however, the ^{22}Ne/^{20}Ne ratios are considerably higher than atmospheric in the 800°C and 1200°C steps of 09MUT08 and 09MUT12. This could be due to strong isotope fractionation in the small fraction of ~3-4% of total Ne retained after the 600°C step (Table A3). On the other hand, a contribution of nucleogenic ^{22}Ne produced by $^{19}F(\alpha,n)^{22}Na(\beta^{+})^{22}Ne$ cannot be excluded. As cosmogenic Ne is typically degassed up to 800°C from quartz (Niedermann, 2002), we have calculated total cosmogenic ^{21}Ne concentrations by summing up the ^{21}Ne excesses up to 800°C, but only including 50±50% of the 800°C contributions (which are small anyway) for 09MUT08 and 09MUT12.

References for Supplementary Material

Desilets, D., Zreda, M., Prabu, T., 2006. Extended scaling factors for in situ cosmogenic nuclides: new measurements at low latitude. Earth Planet. Sci. Lett. 246, 265-276.

Dunai, T., 2001. Influence of secular variation of the magnetic field on production rates of in situ produced cosmogenic nuclides. Earth Planet. Sci. Lett. 193, 197-212.

Kohl, C.P., Nishiizumi, K., 1992. Chemical isolation of quartz for measurement of in situ-produced cosmogenic nuclides. Geochimica et Cosmochimica Acta 56, 3583-3587.

Lifton, N., Bieber, J., Clem, J., Duldig, M., Evenson, P., Humble, J., Pyle, R., 2005. Addressing solar modulation and long-term uncertainties in scaling secondary cosmic rays for in situ cosmogenic nuclide applications. Earth Planet. Sci. Lett. 239, 140-161.

Niedermann, S., 2002. Cosmic-ray-produced noble gases in terrestrial rocks: Dating tools for surface processes. Reviews in Mineralogy and Geochemistry 47, 731-784.

Niedermann, S., Bach, W., Erzinger, J., 1997. Noble gas evidence for a lower mantle component in MORBs from the southern East Pacific Rise: Decoupling of helium and neon isotope systematics. Geochimica et Cosmochimica Acta 61, 2697-2715.

Von Blanckenburg, F., Hewawasam, T., Kubik, P.W., 2004. Cosmogenic nuclide evidence for low weathering and denudation in the wet, tropical highlands of Sri Lanka. J. Geophys. Res. 109, F03008, doi: 10.1029/2003JF000049.

Sample locations and cosmogenic nuclide concentration measurements.

Sample	Latitude (DD)	Longitude (DD)	Elevation (m)	Thickness[a] correction	^{10}Be (10^5 atoms/g)		1σ error (10^5 atoms/g)	^{26}Al (10^5 atoms/g)		1σ error (10^5 atoms/g)	^{26}Al/^{10}Be		Error
08TSERM04	36.5216	33.5052	165	0.979	5.39	±	0.12		n/a			n/a	
08TSERM07	36.6264	33.3680	153	0.979	1.78	±	0.04	13.1	±	1.9	7.4	±	1.1
09MUT05	36.6657	33.3656	154	0.979	1.10	±	0.12	6.0	±	1.3	5.5	±	1.2
09MUT07	36.5342	33.4503	135	0.979		n/a		21.6	±	3.1		n/a	
09MUT08	36.5434	33.4650	179	0.979		n/a		28.6	±	2.0		n/a	
09MUT09	36.5367	33.4579	165	0.979		n/a		27.7	±	2.0		n/a	
09MUT10	36.5527	33.4359	134	0.979	5.16	±	0.04	28.7	±	5.4	5.6	±	1.1
09MUT11	36.5556	33.4389	129	0.979		n/a		22.0	±	5.3		n/a	
09MUT12	36.5492	33.4381	148	0.979	4.17	±	0.03	32.6	±	5.8	7.8	±	1.4
09MUT14	36.5447	33.4454	143	0.979	4.01	±	0.11	24.7	±	5.1	6.2	±	1.3
09MUT15	36.5456	33.4465	128	0.979	4.21	±	0.18	23.6	±	2.1	5.6	±	0.5
09MUT16	36.5283	33.4617	101	0.979	1.63	±	0.19	8.2	±	2.0	5.0	±	1.2
09MUT17	36.5030	33.5187	180	0.979	3.84	±	0.10	19.9	±	1.8	5.2	±	0.5
09MUT18	36.5030	33.5215	205	0.979	6.31	±	0.04	31.6	±	2.1	5.0	±	0.4
ZIY-0	37.0753	35.3503	188	0.975	3.21	±	0.09		n/a			n/a	
ZIY-30	37.0753	35.3503	188	0.819	2.23	±	0.14		n/a			n/a	
ZIY-100	37.0753	35.3503	187	0.562	1.31	±	0.04		n/a			n/a	
ZIY-200	37.0753	35.3503	186	0.363	0.946	±	0.043		n/a			n/a	

n/a means "Not available"; for ^{10}Be measurements, this was due to weak or no current on the AMS. Not all samples were prepared for ^{26}Al measurements.

[a] Thickness correction factor based on sample thickness or depth below surface; topographic shielding was negligible for all samples.

Table A2
Terrace gravel ^{10}Be and ^{26}Al exposure ages from various scaling schemes calculated with the Cronus online calculator*

Sample	^{10}Be Age[a] (ka)	2σ (ka)	^{26}Al Age[a] (ka)	2σ (ka)	^{10}Be Age[b] (ka)	2σ (ka)	^{26}Al Age[b] (ka)	2σ (ka)	^{10}Be Age[c] (ka)	2σ (m)	^{26}Al Age[c] (ka)	2σ (ka)	^{10}Be Age[d] (ka)	2σ (ka)	^{26}Al Age[d] (ka)	2σ (ka)	^{10}Be Age[e] (ka)	2σ (ka)	^{26}Al Age[e] (ka)	2σ (m)	Height (m)	2σ (m)
08TSERM04	120	15	n/a		118	15	n/a		117	12	n/a		111	10	n/a		116	11	n/a		95	6
08TSERM07	40	5	44	8	40	5	43	8	40	4	43	8	37	3	40	7	38	3	42	7	34	3
09MUT05	26	3	21	5	25	3	21	5	25	3	21	5	23	2	19	4	23	2	19	4	31	3
09MUT07	n/a		74	14	n/a		73	14	n/a		73	13	n/a		68	12	n/a		70	12	40	4
09MUT08	n/a		94	13	n/a		92	13	n/a		92	12	n/a		86	10	n/a		89	10	105	6
09MUT09	n/a		94	14	n/a		92	13	n/a		92	12	n/a		86	10	n/a		89	11	70	6
09MUT10	118	15	99	23	116	14	97	23	115	12	97	22	109	9.7	91	20	114	10	95	21	54	6
09MUT11	n/a		76	21	n/a		75	21	n/a		75	20	n/a		70	18	n/a		72	19	43	4
09MUT12	95	12	111	25	93	12	109	25	93	10	109	23	87	8	102	21	91	9	107	22	71	6
09MUT14	92	12	85	21	90	12	83	21	90	10	83	20	84	8	78	18	88	9	81	19	68	6
09MUT15	98	12	82	13	96	12	80	12	96	10	80	11	90	8	75	9	93	9	78	10	53	6
09MUT16	39	5	30	8	38.2	5	29	8	38	4	29	8	35	3	27	7	36	3	27	7	28	3
09MUT17	85	10	66	10	83	10	65	10	83	9	65	9	78	7	60	8	81	7	62	8	110	6
09MUT18	136	17	103	15	133	16	101	14	132	14	101	13	125	11	94	11	132	12	99	11	135	6

* Wrapper script version 2.2, main calculator version 2.1, constants version 2.2.1, muons version 1.1 ; errors represent "external" uncertainties.

[a] Desilets et al. (2006) time-dependent production.

[b] Dunai (2001) time-dependent production.

[c] Lifton et al. (2005) time-dependent production.

[d] Lal (1991)/Stone (2000) time-dependent production.

[e] Lal (1991)/Stone (2000) constant production.

Table A3
Results of Ne analyses in chert separates from three strath terraces. Error limits are 2σ.

Sample	T	^{20}Ne (10^{-12} cm^3 STP/g)	$^{22}Ne/^{20}Ne$	$^{21}Ne/^{20}Ne$	$^{21}Ne_{ex}$[a]
Weight	(°C)		(10^{-2})	(10^{-2})	(10^6 atoms/g)
08TSERM04	400	18.9 ± 1.2	10.32 ± 0.16	0.334 ± 0.027	0.19 ± 0.13
0.70624 g	600	400 ± 24	10.153 ± 0.036	0.3203 ± 0.0055	2.62 ± 0.60
	800	562 ± 33	10.226 ± 0.052	0.3069 ± 0.0053	1.67 ± 0.81
	1200	67.8 ± 4.1	10.401 ± 0.083	0.309 ± 0.012	0.24 ± 0.22
	Total	1049 ± 41	10.221 ± 0.032	0.3126 ± 0.0037	**4.5 ± 1.0**
0.80006 g	crushed	564 ± 40	10.133 ± 0.041	0.2950 ± 0.0052	n/a
09MUT08	400	332 ± 17	10.150 ± 0.064	0.3018 ± 0.0068	0.52 +0.61 - 0.52
0.70150 g	600	897 ± 46	10.244 ± 0.041	0.3038 ± 0.0063	1.9 ± 1.5
	800	34.4 ± 1.9	10.70 ± 0.28	0.330 ± 0.027	0.32 ± 0.17
	1200	0.96 ± 0.41	14.0 ± 1.2	0.80 ± 0.23	0.130 ± 0.046
	Total	1264 ± 49	10.235 ± 0.035	0.3044 ± 0.0049	**2.7 ± 1.6**
09MUT12	400	240 ± 12	10.244 ± 0.084	0.3054 ± 0.0073	0.61 ± 0.47
0.71772 g	600	269 ± 14	10.453 ± 0.074	0.3172 ± 0.0059	1.55 ± 0.44
	800	12.1 ± 1.1	10.91 ± 0.25	0.329 ± 0.025	0.108 ± 0.081
	1200	10.02 ± 0.65	10.99 ± 0.28	0.376 ± 0.033	0.216 ± 0.087
	Total	531 ± 18	10.379 ± 0.054	0.3132 ± 0.0045	**2.21 ± 0.70**
1.00102 g	crushed	31.0 ± 2.3	10.32 ± 0.13	0.301 ± 0.015	n/a

[a] Excess ^{21}Ne over atmospheric abundances. Totals show estimated concentration of cosmogenic ^{21}Ne, calculated based on the excesses in the 400 to 800 °C steps (see text in Supplementary Material).

Table A4

Exposure ages calculated from ^{21}Ne analyses and terrace heights above thalweg.

Sample	^{21}Ne (10^6 atoms/g)	2 σ error (10^6 atoms/g)	^{10}Be prod. rate (atoms/(g*yr))	^{21}Ne prod. rate[a] (atoms/(g*yr))	Exposure age[b] (ka)	Height (m)
09MUT08	2.7	1.6	4.832	21.3 ± 2.2	130 ± 78	105
08TSERM04	4.5	1.0	4.771	21.0 ± 2.2	219 ± 54	95
09MUT12	2.21	0.70	4.700	20.7 ± 2.2	109 ± 36	71

[a] 2σ error includes uncertainty in $^{10}Be/^{21}Ne$ production rate ratio and estimated 10% uncertainty in ^{10}Be production rate.
[b] 2σ error includes uncertainty in ^{21}Ne production rate and ^{21}Ne concentration measurement.

Table A5

Estimations of cosmogenic ^{10}Be inherited component of Adana terrace.

Erosion rate (m/Myr)	Minimized χ^2	Surface age (a)	Inherited component (atoms/g)
Assuming density = 1.8 g/cm^3			
4	0.328	55,926	88,250
6	0.319	60,110	88,340
8	0.308	65,282	88,450
10	0.294	71,919	88,595
12	0.276	80,918	88,795
Assuming density = 2.0 g/cm^3			
4	1.98	56,529	90,460
6	1.95	61,398	90,520
8	1.92	67,630	90,700
10	1.87	76,042	90,900
11.5	1.82	84,768	91,100